Received April 19, 2018, accepted May 17, 2018, date of publication May 22, 2018, date of current version June 26, 2018.

Digital Object Identifier 10.1109/ACCESS.2018.2839642

Limit Cycle Elimination in Inverted Pendulums: Furuta Pendulum and Pendubot

MAYRA ANTONIO-CRUZ[1], VICTOR MANUEL HERNÁNDEZ-GUZMÁN[2], AND RAMÓN SILVA-ORTIGOZA[1]

[1]Área de Mecatrónica, CIDETEC, Instituto Politécnico Nacional, Mexico City 07700, Mexico
[2]Facultad de Ingeniería, Universidad Autónoma de Querétaro, Querétaro 76010, Mexico

Corresponding author: Victor Manuel Hernández-Guzmán (vmhg@uaq.mx)

This work was supported by the Secretaría de Investigación y Posgrado del Instituto Politécnico Nacional, México. The work of M. Antonio-Cruz was supported by the CONACYT-México and BEIFI-IPN Scholarships. The work of V. M. Hernández-Guzmán was supported by the SNI-México. The work of R. Silva-Ortigoza was supported by the SNI-México and the IPN programs EDI and COFAA.

ABSTRACT This paper presents the design of a linear state feedback controller for the stabilization of two inverted pendulums, namely, Furuta pendulum and pendubot. Such a controller design allows eliminating the limit cycle that appears in the systems due to the effect of a nonlinearity, that is, dead-zone, which is induced by static friction at the motor shaft. To do this, the differential flatness approach is applied to the linear approximate model of the inverted pendulums under study. Then, the resulting flat systems are translated to the frequency domain for which a control scheme is proposed. Subsequently, the dead-zone nonlinearity is treated off-line as an approximation obtained through the describing function method. Since this is an approach intrinsically based on frequency response, the frequency response-based approach is suitable for tuning the gains of the proposed control scheme. An advantage of using the frequency response-based approach along with the describing function method is that they allow obtaining precise formulas that simplify the tuning of the proposed control scheme, so that the limit cycle caused by the dead-zone is eliminated. This must be contrasted with a time response-based approach, proposed recently by the authors, where precise formulas were not obtained and intuitive ideas have to be used to eliminate limit cycle. Finally, the procedure of the controller design herein proposed is verified via experimental tests.

INDEX TERMS Inverted pendulum, Furuta pendulum, pendubot, stabilization, state feedback control, differential flatness, dead-zone, frequency response, describing function, limit cycle.

I. INTRODUCTION

There are several control schemes designed to stabilize inverted pendulums [1]–[3]. With the accelerated development of technology such control schemes are demanded to have a better performance. Thus, stabilization control designs dealing with uncertainties and external disturbances [4]–[7], unknown parameters, models, and velocities [8]–[10], friction compensation [11]–[14], etc. have been reported. It is well known that in inverted pendulums, and in all control systems involving mechanical motion, the control performance also degrades by the presence of nonlinearities, such as backlash [15], [16], dead-zone [17], [18], rolling friction, drive-train friction, and sensor bandwidth, among other. These nonlinearities cause limit cycle phenomenon or even instability in the system [19].

Regarding limit cycles generated by friction and stiction in control systems, there are different contributions [20]–[25]. In particular, the limit cycle in stabilization control of inverted pendulums have been reported in different papers [26]–[33]. However, most of the papers are focused on generation and behavior study of stable limit cycles and only two of them treat the reduction [30] and elimination [32] of limit cycle caused by nonlinearities. Also, most of the papers ([20], [21], [23]–[31]) use advanced control techniques, such as: dual-relay feedback approach, negative stiffness control, bifurcation analysis, asymptotic solutions, sliding mode approach, partial nonlinear feedback linearization and dynamic control, passivity-based and nonlinear observers, and Jacobian Poincaré maps. Thus, [32] is interesting because it shows that a simple linear state feedback controller suffices for limit cycle elimination. There, a suitable tuning procedure based on linear system differential flatness, describing function, and classical control, i.e., root locus, was introduced. Hence, the main ideas are simple compared with the advanced control techniques introduced in the above cited papers. Despite this, procedure in [32] has the drawback that controller design

relies on the time response of the system; whereas the describing function method is an approach intrinsically based on frequency response. This implies that procedure in [32] does not provide precise formulas, so that intuitive ideas had to be used to eliminate limit cycle. On the other hand, it is important to remark that some authors [11] have reported that oscillatory behavior induced by static friction, i.e., dead-zone nonlinearity [34], in a Furuta pendulum remains in spite of modifying the parameters of the control system. Finally, other papers dealing with performance improvement of inverted pendulums have been reported [35]–[38].

Based on the previous literature review, it is evident that procedures to mitigate the effects of nonlinearities are needed to improve the performance of control systems. In that direction, contribution of the present paper is introducing a frequency response-based solution for problem described in [32]. As a result and despite that, similarly as in [32], the controller gains that eliminate the limit cycle are still found via an iterative experimental procedure, several precise formulas are obtained in the present paper. These formulas render easier selection of the controller gains and commissioning of experimental procedure for the limit cycle elimination in the Furuta pendulum and pendubot.

This paper is organized as follows. Section II presents the differential parametrization of the Furuta pendulum and pendubot. In Section III a control scheme is proposed to stabilize those systems, facing the static friction-induced dead-zone nonlinearity. Procedure to select gains of the control scheme is given in Section IV, which is extended in Section V to experimentally eliminate dead-zone nonlinearity-induced limit cycle. Also, Section V details advantages with regards to controller design reported in [32]. Lastly, Section VI gives the conclusion.

II. FURUTA PENDULUM AND PENDUBOT LINEAR MODELS

This section presents the linear approximate model as well as the corresponding differential flatness model of the inverted pendulums under study, that is, Furuta pendulum and pendubot.

A. DESCRIPTION OF THE SYSTEMS

On the one hand, the Furuta pendulum mechanism is essentially composed by a motor and two bars called *arm* and *pendulum*. Motor shaft is fixed at one end of the arm, producing arm angular movement in a horizontal plane. While, pendulum is placed at the free end of the arm by means of a joint allowing rotation of pendulum in a vertical plane orthogonal to arm. On the other hand, the pendubot is mainly composed for two rigid bars and a motor. The motor is fixed at one end of one bar, the free end of this bar is interconnected with the other bar by a rotational join. The motion of both bars is in the vertical plane. In the remainder of the paper bar connected to the motor shall be called *bar A*, while bar connected to this latter shall be called *bar B*.

The mechanisms above described as well as its corresponding variables and parameters are shown in Fig. 1. There,

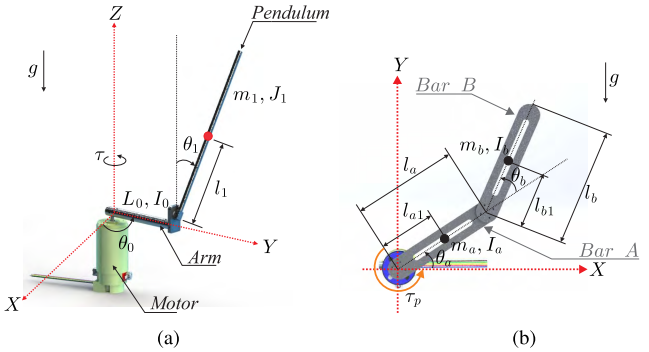

FIGURE 1. Diagrams of the inverted pendulums under study. (a) Furuta pendulum. (b) Pendubot.

for the Furuta pendulum, θ_0 and θ_1 are the arm angular position measured with respect to an arbitrary position and the pendulum angular position measured with respect to the upright position, respectively, τ denotes the torque generated by the motor and applied to arm, I_0 stands for motor inertia plus arm inertia (when this turns around an axis orthogonal to one of its ends), L_0 corresponds to the arm length. Whereas, m_1, l_1, and J_1 are the mass, center of mass location, and inertia around the center of mass of the pendulum, respectively. Likewise, for the pendubot, θ_a, m_a, I_a, l_a, and l_{a1} are the angular position, mass, inertia, length, and distance to the center of mass of the *bar A*, respectively; whereas θ_b, m_b, I_b, l_b, and l_{b1} are the angular position, mass, inertia, length, and distance to the center of mass of the *bar B*, respectively. τ_P is the torque generated by the motor and applied to the *bar A*. Lastly, g is the acceleration of gravity.

B. LINEAR APPROXIMATE MODELS

The general linear approximate model of a nonlinear system is:

$$\dot{x}_\delta = \mathcal{A}x_\delta + \mathcal{B}u_\delta, \tag{1}$$

where x_δ is the incremental state vector, $\mathcal{A}$ and $\mathcal{B}$ are constant matrices, and u_δ is the incremental input of the system. Such a linear approximate model is valid only around the constant operation point $\overline{x}$ with the constant input $\overline{u}$.

In [43] and [44] it was shown that (1) for the Furuta pendulum has the following definitions:

$$\begin{aligned} x_\delta &= \begin{bmatrix} x_{\delta 1} \\ x_{\delta 2} \\ x_{\delta 3} \\ x_{\delta 4} \end{bmatrix} = \begin{bmatrix} \theta_0 - \overline{\theta}_0 \\ \dot{\theta}_0 - \dot{\overline{\theta}}_0 \\ \theta_1 - \overline{\theta}_1 \\ \dot{\theta}_1 - \dot{\overline{\theta}}_1 \end{bmatrix}, \quad u_\delta = \tau - \overline{\tau} = \tau, \\ \mathcal{A} &= \begin{bmatrix} 0 & 1 & 0 & 0 \\ 0 & 0 & a_{23} & 0 \\ 0 & 0 & 0 & 1 \\ 0 & 0 & a_{43} & 0 \end{bmatrix}, \quad \mathcal{B} = \begin{bmatrix} 0 \\ b_{21} \\ 0 \\ b_{41} \end{bmatrix}, \end{aligned} \tag{2}$$

with

$$\begin{aligned} a_{23} &= \frac{-gm_1^2 l_1^2 L_0}{I_0\left(J_1 + m_1 l_1^2\right) + J_1 m_1 L_0^2}, \\ a_{43} &= \frac{\left(I_0 + m_1 L_0^2\right) m_1 l_1 g}{I_0\left(J_1 + m_1 l_1^2\right) + J_1 m_1 L_0^2}, \\ b_{21} &= \frac{J_1 + m_1 l_1^2}{I_0\left(J_1 + m_1 l_1^2\right) + J_1 m_1 L_0^2}, \\ b_{41} &= \frac{-m_1 l_1 L_0}{I_0\left(J_1 + m_1 l_1^2\right) + J_1 m_1 L_0^2}, \end{aligned} \tag{3}$$

around the operation point:

$$\begin{aligned} &\overline{x} = \begin{bmatrix} \overline{\theta}_0 & \overline{\dot{\theta}}_0 & \overline{\theta}_1 & \overline{\dot{\theta}}_1 \end{bmatrix}^T = \begin{bmatrix} 0 & 0 & 0 & 0 \end{bmatrix}^T, \\ &\overline{u} = \overline{\tau} = 0. \end{aligned} \tag{4}$$

It is useful to know that the approximate model (1) for the Furuta pendulum is also valid if $\overline{\theta}_1 = \pm 2\pi$.

Also in [43] and [44] it was obtained that (1) for the pendubot has the following redefinitions of (2), (3), and (4):

$$\begin{aligned} x_\delta &= \begin{bmatrix} x_{\delta 1} \\ x_{\delta 2} \\ x_{\delta 3} \\ x_{\delta 4} \end{bmatrix} = \begin{bmatrix} \theta_a - \overline{\theta}_a \\ \dot{\theta}_a - \overline{\dot{\theta}}_a \\ \theta_b - \overline{\theta}_b \\ \dot{\theta}_b - \overline{\dot{\theta}}_b \end{bmatrix}, \quad u_\delta = \tau_P - \overline{\tau}_P, \\ \mathcal{A} &= \begin{bmatrix} 0 & 1 & 0 & 0 \\ a_{21} & 0 & a_{23} & 0 \\ 0 & 0 & 0 & 1 \\ a_{41} & 0 & a_{43} & 0 \end{bmatrix}, \quad \mathcal{B} = \begin{bmatrix} 0 \\ b_{21} \\ 0 \\ b_{41} \end{bmatrix}, \end{aligned} \tag{5}$$

with (3) redefined as

$$\begin{aligned} a_{21} &= \frac{\left(\alpha_2\alpha_4 - \alpha_3\alpha_5\right) g}{\alpha_1\alpha_2 - \alpha_3^2}, \\ a_{23} &= -\frac{\alpha_3\alpha_5 g}{\alpha_1\alpha_2 - \alpha_3^2}, \\ a_{41} &= \frac{\left(\alpha_1 + \alpha_3\right)\alpha_5 g - \left(\alpha_2 + \alpha_3\right)\alpha_4 g}{\alpha_1\alpha_2 - \alpha_3^2}, \\ a_{43} &= \frac{\left(\alpha_1 + \alpha_3\right)\alpha_5 g}{\alpha_1\alpha_2 - \alpha_3^2}, \\ b_{21} &= \frac{\alpha_2}{\alpha_1\alpha_2 - \alpha_3^2}, \\ b_{41} &= \frac{-\alpha_2 - \alpha_3}{\alpha_1\alpha_2 - \alpha_3^2}, \end{aligned} \tag{6}$$

where

$$\begin{aligned} &\alpha_1 = m_a l_{a1}^2 + I_a + m_b l_a^2, \quad \alpha_2 = m_b l_{b1}^2 + I_b, \\ &\alpha_3 = m_b l_{b1} l_a, \quad \alpha_4 = m_a l_{a1} + m_b l_a, \quad \alpha_5 = m_b l_{b1}, \end{aligned}$$

around the redefined operation point:

$$\begin{aligned} &\overline{x} = \begin{bmatrix} \overline{\theta}_a & \overline{\dot{\theta}}_a & \overline{\theta}_b & \overline{\dot{\theta}}_b \end{bmatrix}^T = \begin{bmatrix} \frac{\pi}{2} & 0 & 0 & 0 \end{bmatrix}^T, \\ &\overline{u} = \overline{\tau}_P = 0. \end{aligned} \tag{7}$$

C. DIFFERENTIAL FLATNESS MODELS

In [32] and [39] it was determined that (1) with (2) and (3) is differentially flat [40, Ch. 2]. Hence, it was shown in [32] that the following flat output, F, and differential parametrization is obtained for the Furuta pendulum:

$$F = x_{\delta 1} + h x_{\delta 3}, \tag{8}$$

$$\dot{F} = x_{\delta 2} + h x_{\delta 4}, \tag{9}$$

$$\ddot{F} = (a_{23} + a_{43} h) x_{\delta 3}, \tag{10}$$

$$F^{(3)} = (a_{23} + a_{43} h) x_{\delta 4}, \tag{11}$$

$$F^{(4)} = a_{43}\ddot{F} + b_{41}(a_{23} + a_{43} h)\tau, \tag{12}$$

where

$$h = \frac{J_1 + m_1 l_1^2}{L_0 l_1 m_1}.$$

In the pendubot case, since the determinant of its controllability matrix, $\mathcal{C}$, is obtained by using (5) and (6) as follows:

$$\begin{aligned} \det \mathcal{C} &= \det \begin{bmatrix} \mathcal{B} & \mathcal{A}\mathcal{B} & \mathcal{A}^2\mathcal{B} & \mathcal{A}^3\mathcal{B} \end{bmatrix}, \\ &= \det \begin{bmatrix} 0 & b_{21} & 0 & a_{21}b_{21} + a_{23}b_{41} \\ b_{21} & 0 & a_{21}b_{21} + a_{23}b_{41} & 0 \\ 0 & b_{41} & 0 & a_{41}b_{21} + a_{43}b_{41} \\ b_{41} & 0 & a_{41}b_{21} + a_{43}b_{41} & 0 \end{bmatrix}, \\ &= \frac{\alpha_5^2\alpha_3^2 g^2}{\left(\alpha_1\alpha_2 - \alpha_3^2\right)^4}, \end{aligned}$$

which is different to zero, therefore (1) with (5) and (6) is controllable and, in consequence, differentially flat [40]. Thus, the flat output of the pendubot is given by

$$F_P = \lambda \begin{bmatrix} 0 & 0 & 0 & 1 \end{bmatrix} \mathcal{C}^{-1} x_\delta, \tag{13}$$

where λ is an arbitrary nonzero constant, conveniently chosen as:

$$\lambda = (c_2 b_{21} - c_1 b_{41})\left(\alpha_1\alpha_2 - \alpha_3^2\right),$$

with

$$\begin{aligned} c_1 &= \frac{\alpha_2^2\alpha_4 g + \alpha_3^2\alpha_5 g^2}{\left(\alpha_1\alpha_2 - \alpha_3^2\right)^2}, \\ c_2 &= \frac{\alpha_2\alpha_4\left(\alpha_2 - \alpha_3\right) g - \alpha_3\alpha_5\left(\alpha_1 + \alpha_3\right) g}{\left(\alpha_1\alpha_2 - \alpha_3^2\right)^2}. \end{aligned}$$

After calculations, F_P and its first four time derivatives are determined by

$$F_P = x_{\delta 1} + \frac{\alpha_2}{\alpha_2 + \alpha_3} x_{\delta 3}, \tag{14}$$

$$\dot{F}_P = x_{\delta 2} + \frac{\alpha_2}{\alpha_2 + \alpha_3} x_{\delta 4}, \tag{15}$$

$$\ddot{F}_P = \frac{\alpha_5 g}{\alpha_2 + \alpha_3}\left(x_{\delta 1} + x_{\delta 3}\right), \tag{16}$$

$$F_P^{(3)} = \frac{\alpha_5 g}{\alpha_2 + \alpha_3}\left(x_{\delta 2} + x_{\delta 4}\right), \tag{17}$$

$$\begin{aligned} F_P^{(4)} = &\left(\frac{\alpha_1\alpha_5 + \alpha_2\alpha_4}{\alpha_1\alpha_2 - \alpha_3^2}\right) g\ddot{F} - \frac{\alpha_4\alpha_5}{\alpha_1\alpha_2 + \alpha_3^2} g^2 F \\ &- \frac{\alpha_3\alpha_5}{\left(\alpha_2 + \alpha_3\right)\left(\alpha_1\alpha_2 - \alpha_3^2\right)} \tau_P. \end{aligned} \tag{18}$$

The expressions (12) and (18) represent the differential flat model that describes the dynamics (1) for the Furuta pendulum and pendubot, respectively.

III. LINEAR STATE FEEDBACK CONTROL

A linear control scheme for stabilization of the Furuta pendulum and pendubot mechanisms is proposed in this section. This control is derived by using the flat models (12) and (18). Furthermore, such a control scheme is studied under the effect of a dead-zone nonlinearity induced by static friction at the shaft of the actuator in each system.

A. PROPOSING THE CONTROL SCHEME

It is shown in [32] that, by applying Laplace transform to (12), the following transfer function is equivalent to (1) with (2) and (3) around the operation point (4):

$$G_F(s) = \frac{F(s)}{\tau(s)} = \frac{b_{41}(a_{23} + a_{43}h)}{s^2(s^2 - a_{43})}, \tag{19}$$

where $F(s)$ and $\tau(s)$ stand for Laplace transforms of flat output and applied torque of the Furuta pendulum, respectively. Poles of this transfer function are real located at $s = 0$ (two of them), one at $s = -\sqrt{a_{43}} < 0$, and another at $s = \sqrt{a_{43}} > 0$. It is stressed that a_{43} is a positive real number.

Proceeding similarly for the pendubot, by applying Laplace transform to (18) it is found that the following transfer function is equivalent to (1) with (5) and (6) around the operation point (7):

$$G_P(s) = \frac{F_P(s)}{\tau_P(s)} = \frac{-n_P}{s^4 - n_P s^2 + m_P}, \tag{20}$$

where $F_P(s)$ and $\tau_P(s)$ are the Laplace transforms of flat output and applied torque of the pendubot, respectively, and

$$n_P = \frac{\alpha_3\alpha_5 g}{(\alpha_2 + \alpha_3)\left(\alpha_1\alpha_2 - \alpha_3^2\right)},$$
$$m_P = \frac{\alpha_4\alpha_5 g^2}{\alpha_1\alpha_2 - \alpha_3^2}.$$

Note that $n_P > 0$ for any parameters of the pendubot and that the four poles of (20) are complex conjugate, two of them with positive real part and the other two with negative real part.

Block diagram in Fig. 2 is a slightly modified version of control scheme proposed in [32] to control (19), where a dead-zone nonlinearity is considered. There, α, k_v, k_d, k_p are the control gains. Also, it is not difficult to verify that $b_{41}(a_{23} + a_{43}h) < 0$ for any set of Furuta pendulum parameters.

From Fig. 2, it is clear that control $\tau(s)$ is given by:

$$\tau(s) = k_v F(s) s^3 + \alpha F(s) s^2 + k_d F(s) s + k_p F(s). \tag{21}$$

The same control law is also used to control (20), as represented in Fig. 3. Since $n_P > 0$, $-n_P < 0$ for any parameters of the pendubot. Also, note that the controller in Fig. 3 is realizable because it consists in the feedback of the output of the fourth order plant and its first three time derivatives.

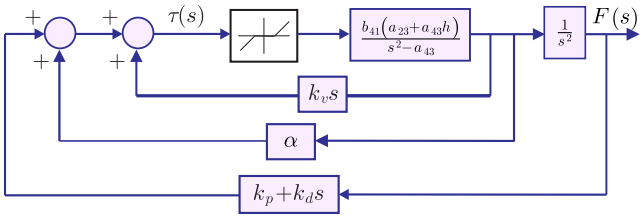

FIGURE 2. Closed-loop system of the Furuta pendulum, considering a dead-zone nonlinearity.

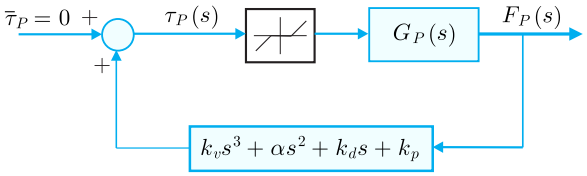

FIGURE 3. Closed-loop system of the pendubot, considering a dead-zone nonlinearity.

When replacing in (21) the differential parametrization of the Furuta pendulum and pendubot, that is, (8)–(12) and (14)–(18), respectively, it is found that the control (21) is equivalent to the following linear state feedback controller:

$$\begin{aligned} u_\delta &= -Kx_\delta, \\ &= -k_1 x_{\delta 1} - k_2 x_{\delta 2} - k_3 x_{\delta 3} - k_4 x_{\delta 4}, \end{aligned} \tag{22}$$

where $K = [k_1, k_2, k_3, k_4]$ is the gain vector and u_δ, x_δ stand, for the case of the Furuta pendulum, as defined in (2) if the below relations are used:

$$\begin{aligned} -k_p &= k_1, \\ -k_d &= k_2, \\ -\left[\alpha\left(a_{23} + a_{43}h\right) + k_p h\right] &= k_3, \\ -\left[k_v\left(a_{23} + a_{43}h\right) + k_d h\right] &= k_4, \end{aligned} \tag{23}$$

and, for the case of the pendubot, as defined in (5) if the following relations are considered:

$$\begin{aligned} -\left(\frac{\alpha\alpha_5 g}{\alpha_2 + \alpha_3} + k_p\right) &= k_1, \\ -\left(\frac{k_v\alpha_5 g}{\alpha_2 + \alpha_3} + k_d\right) &= k_2, \\ -\left(\frac{\alpha\alpha_5 g + \alpha_2 k_p}{\alpha_2 + \alpha_3}\right) &= k_3, \\ -\left(\frac{k_v\alpha_5 g + \alpha_2 k_d}{\alpha_2 + \alpha_3}\right) &= k_4. \end{aligned} \tag{24}$$

B. THE DESCRIBING FUNCTION APPROACH

It is suggested in [41, Ch. 5], to represent the closed-loop systems in Figs. 2 and 3 in the standard form shown in Fig. 4. This is carried out applying block algebra on Figs. 2 and 3. The nonlinearity input being $e = \tau(s)$ for the case of the Furuta pendulum and $e = \tau_P(s)$ for the pendubot, while the linear time invariant system $G(s)$ is:

$$G(s) = G_1(s) G_2(s), \tag{25}$$

where $G_1(s) = \frac{-b_{41}(a_{23}+a_{43}h)}{s^2(s^2-a_{43})}$, with $-b_{41}(a_{23}+a_{43}h) > 0$, when treating the Furuta pendulum or $G_1(s) = \frac{-(-n_P)}{s^4-n_P s^2+m_P}$, with $-(-n_P) > 0$, when attending the pendubot, and $G_2(s) = k_v s^3 + \alpha s^2 + k_d s + k_p$ is the controller. Note that $G(s)$ in both the Furuta pendulum and pendubot has four poles and only three zeros, i.e., magnitude of (25) behaves as a low-pass filter, which is needed to apply the describing function method.

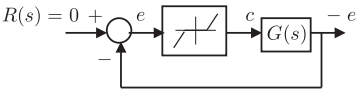

FIGURE 4. Equivalent representation of block diagrams in Figs. 2 and 3.

The describing function of a dead-zone nonlinearity is an approximate frequency response description, which is given by [41, Ch. 5]:

$$N(A) = \frac{2k}{\pi}\left[\frac{\pi}{2} - \sin^{-1}\left(\frac{\delta}{A}\right) - \frac{\delta}{A}\sqrt{1-\left(\frac{\delta}{A}\right)^2}\right], \quad (26)$$

if $A \geq \delta$, where the dead-zone is located at the interval $e \in [-\delta, \delta]$ and k is the nonlinearity slope outside this interval. It is assumed that the nonlinearity input e is a sinusoidal function of time with amplitude A and frequency ω. "Transfer function" $N(A)$ is real, positive, frequency independent but dependent on the input amplitude A. Its maximal value is $N(A) = k > 0$, which is reached as $A \to \infty$, and its minimal value tends to zero if $A \to \delta$. A limit cycle may exist if [41, Ch. 5]:

$$G(j\omega) = -\frac{1}{N(A)}. \quad (27)$$

In other words, a limit cycle may exist if polar plot of $G(j\omega)$ intersects the negative real axis in the open interval $(-\infty, -1/k)$. This latter is true since $N(A)$ is real and positive, which implies that $-1/N(A)$ is real and negative. The oscillation frequency, ω_σ, and amplitude of the oscillation are found as the values of ω, in $G(j\omega)$, and A, in $-1/N(A)$, at point σ where their plots intersect [41, Ch. 5]. A graphic representation of this idea is depicted in Fig. 5.

IV. PROCEDURE FOR SELECTING THE CONTROL GAINS

Selection of the control gains k_v, α, k_d, and k_p can be performed as explained in the following.

For the Furuta pendulum, recalling Fig. 2 and omitting the dead-zone nonlinearity, the transfer function of the two internal loops can be obtained as:

$$\frac{b_{41}(a_{23}+a_{43}h)}{s^2 - b_{41}(a_{23}+a_{43}h)k_v s - (a_{43}+\alpha b_{41}(a_{23}+a_{43}h))}. \quad (28)$$

Note that, since $b_{41}(a_{23}+a_{43}h) < 0$, ensuring all coefficients of characteristic polynomial in (28) to be positive requires to choose positive values for k_v and α and, also, α must be large enough so that $a_{43} < |\alpha b_{41}(a_{23}+a_{43}h)|$.

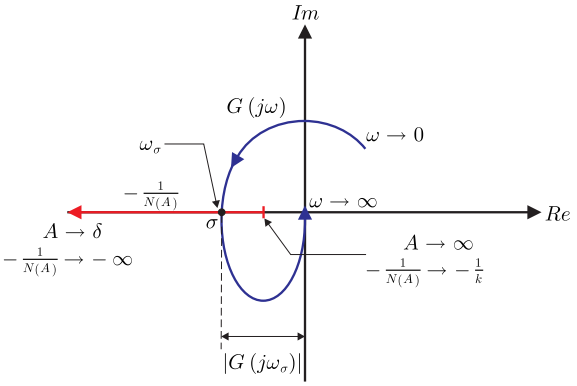

FIGURE 5. Polar plot of $G(j\omega)$ and $-1/N(A)$.

For the pendubot, when considering Fig. 3 and neglecting the dead-zone nonlinearity, the following transfer function in closed-loop is obtained:

$$\frac{-n_P}{s^4 + n_P k_v s^3 + a_1 s^2 + n_P k_d s + a_2}, \quad (29)$$

where

$$a_1 = n_P\alpha - \left(\frac{\alpha_1\alpha_5 + \alpha_2\alpha_4}{\alpha_1\alpha_2 - \alpha_3^2}\right)g,$$
$$a_2 = m_P + n_P k_p,$$

from which it is obtained that

$$k_v > 0, \quad (30)$$
$$\alpha > 0 \quad \wedge \quad n_P\alpha > \frac{\alpha_1\alpha_5 + \alpha_2\alpha_4}{\alpha_1\alpha_2 - \alpha_3^2}, \quad (31)$$
$$k_d > 0,$$
$$k_p > 0$$

are necessary to ensure all coefficients of characteristic polynomial in (29) to be positive. Hence, conditions (30) and (31) are used to choose k_v and α for the controller of the pendubot.

With k_v and α chosen as indicated for the Furuta pendulum and pendubot, in both cases k_d and k_p can be selected by considering the following:

a) Note that $-b_{41}(a_{23}+a_{43}h) > 0$ and $-(-n_P) > 0$, hence, phase of $G_1(j\omega)$ is $-360°$ for all $\omega \geq 0$. This can be verified by replacing s by $j\omega$ in $G_1(s)$ for the Furuta pendulum and pendubot.

b) Replacing s by $j\omega$ in $G_2(s)$ it is found:

$$G_2(j\omega) = k_v(j\omega)^3 + \alpha(j\omega)^2 + k_d(j\omega) + k_p,$$
$$= j\left(k_d\omega - k_v\omega^3\right) + \left(k_p - \alpha\omega^2\right),$$

whose magnitude is given as,

$$|G_2(j\omega)| = \sqrt{\left(k_d\omega - k_v\omega^3\right)^2 + \left(k_p - \alpha\omega^2\right)^2}. \quad (32)$$

Solving (32) for k_p, it is obtained:

$$k_p = \pm\sqrt{|G_2(j\omega)|^2 - \left(k_d\omega - k_v\omega^3\right)^2} + \alpha\omega^2. \quad (33)$$

c) In order to force the polar plot of $G(j\omega)$ to intersect the negative real axis, i.e., to render phase of $G(j\omega)$ equal to $-180°$ at some $\omega > 0$, phase of $G_2(j\omega)$ must be $+180°$ for the same ω (see a) above), that is:

$$\angle G_2(j\omega) = \arctan\left(\frac{k_d\omega - k_v\omega^3}{k_p - \alpha\omega^2}\right) = +180. \quad (34)$$

This is satisfied if,

$$k_p - \alpha\omega^2 < 0, \quad (35)$$

$$k_d\omega - k_v\omega^3 = 0. \quad (36)$$

Therefore, sign in (33) has to be chosen so that (35) is accomplished.

d) From (36) the following relation to find k_d is obtained:

$$k_d = k_v\omega^2. \quad (37)$$

Note that to find k_p and k_d, it is necessary to propose the frequency $\omega = \omega_\sigma$ at which it is desired that polar plot of $G(j\omega)$ intersects the negative real axis. Also, the magnitude $|G_2(j\omega_\sigma)|$ that must be introduced by the control has to be known. To this end, a desired magnitude for $G(j\omega)$ when $\omega = \omega_\sigma$ has to be proposed. Since:

$$|G(j\omega_\sigma)| = |G_1(j\omega_\sigma)| \cdot |G_2(j\omega_\sigma)|,$$

then

$$|G_2(j\omega_\sigma)| = \frac{|G(j\omega_\sigma)|}{|G_1(j\omega_\sigma)|}. \quad (38)$$

where $|G_1(j\omega_\sigma)|$ can be obtained from Bode diagrams of $G_1(j\omega)$. Thus, Bode diagrams are a suitable tool to design the controller gains k_v, α, k_d, and k_p.

V. EXPERIMENTAL PROCEDURE FOR LIMIT CYCLE ELIMINATION

In this section, the procedure described in Section IV to select the gains of control (21) is extended in order to eliminate the limit cycle that appears in the control systems under study, when a dead-zone nonlinearity is considered. Such an extension is exemplified through iterative experimental tests. Also, advantages of this procedure with regards to the one presented in [32] are given. The following conjecture has been introduced in [32].

A. CONJECTURE

According to the dead-zone nonlinearity characteristic function [32], if $|e| \leq \delta$ then a zero value appears at the plant input $c = 0$, i.e., torque applied by motor to the mechanism is zero and it might rest at the operation point: (4) of the Furuta pendulum or (7) of the pendubot. Since threshold δ is uncertain because static friction is uncertain, it is natural to wonder whether it is possible to render $A < \delta$ in experiments if A is small enough, despite (26) is only valid for $A \geq \delta$. In such a case, mechanism might stay at rest at the operation point if A is chosen to be small enough, i.e., limit cycle might vanish under these conditions.

In the following sections, the above conjecture is tested through experiments.

B. DESCRIPTION OF THE PROTOTYPES

The Furuta pendulum and pendubot prototypes used in the experimental tests are shown in Fig. 6 and were built at the Mechatronics Laboratory of CIDETEC-IPN. These prototypes have four stages: *a) Mechanical structure*, refers to the mechanical elements composing each prototype. *b) Actuator and sensors*, this stage corresponds to DC motor model 14204S006 from Pittman and two incremental encoders used to measure the angular positions of each system. Encoder used to measure the arm position and the *bar A* position is included in the DC motor chassis and has 500 PPR. Encoders for measuring the position of the pendulum and *bar B* are an ITD01A4Y1 model and an ITD01B14 model, respectively, both from Baumer and with 1024 PPR. *c) Power stage*, it is integrated by the HF100W-SF-24 switched power supply and an AZ12A8DDC servo-drive manufactured by Advanced Motion Controls. This latter possesses an inner current-loop driven by a PI controller, which allows to assume that the current flowing through the DC motor terminals reaches the current imposed by the control signal. This means that torque can be used as the control signal. *d) Data acquisition and processing*, this stage corresponds to a DS1104 board from dSPACE, Matlab-Simulink, and ControlDesk through which the controller is implemented and system variables are read. In all experiments, the angular velocities $\dot{\theta}_0$, $\dot{\theta}_1$, $\dot{\theta}_a$, and $\dot{\theta}_b$ were estimated via a derivative block of Simulink and the sampling period was set to 1 ms.

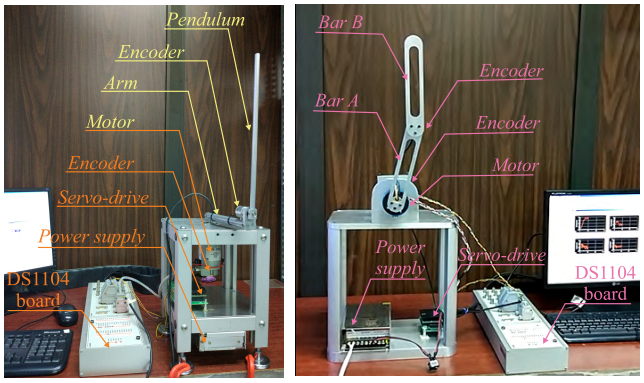

(a) (b)

FIGURE 6. Prototypes built. (a) Furuta pendulum. (b) Pendubot.

The mechanical parameters of the Furuta pendulum and pendubot prototypes are presented in Table 1. They were found by measuring the lengths of the arm, pendulum, *bar A*, and *bar B*, weighing them, and computing the inertias using formulas from Physics [42]. Regarding the numerical value of δ, this was experimentally obtained. The experiments consisted in applying a ramp of torque to the motor of both prototypes, which was set first as $r = mt$ and then as $r = -mt$. For the Furuta pendulum $r = \tau$ and $m = 0.002$ whereas for the pendubot $r = \tau_P$ and $m = 0.016$. The test was repeated several times and the obtained results are depicted in Fig. 7, from which the largest δ was chosen, that is,

$\delta = 8.157 \times 10^{-3}$ for the Furuta pendulum and $\delta = 24.7 \times 10^{-3}$ for the pendubot.

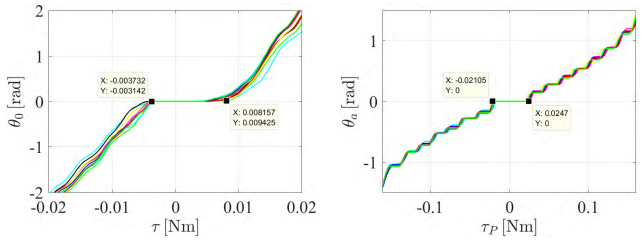

(a) (b)

FIGURE 7. Experimental obtaining of δ. (a) Furuta pendulum. (b) Pendubot.

TABLE 1. Parameters of the prototypes.

Furuta pendulum	Pendubot
$L_0 = 141.4 \times 10^{-3}$ m	$l_a = 200 \times 10^{-3}$ m
$I_0 = 0.4592 \times 10^{-3}$ kg · m^2	$l_b = 200 \times 10^{-3}$ m
$m_1 = 0.038$ kg	$l_{a1} = 100 \times 10^{-3}$ m
$l_1 = 147.5 \times 10^{-3}$ m	$l_{a2} = 100 \times 10^{-3}$ m
$J_1 = 0.2755 \times 10^{-3}$ kg · m^2	$m_a = 0.033$ kg
$k = 1$	$m_b = 0.034$ kg
$\delta = 8.157 \times 10^{-3}$	$I_a = 0.4724 \times 10^{-3}$ kg · m^2
	$I_b = 0.1207 \times 10^{-3}$ kg · m^2
	$k = 1$
	$\delta = 24.7 \times 10^{-3}$

C. EXPERIMENTAL RESULTS

With the parameters in Table 1 the following was found for the Furuta pendulum:

$$b_{41}\,(a_{23} + a_{43}h) = -7.6842 \times 10^4, \quad a_{43} = 93.6678, \quad (39)$$

and for the pendubot:

$$-n_P = -3.7465 \times 10^4. \quad (40)$$

According to conjecture in Section V-A, limit cycle might be avoided if the oscillation amplitude A is chosen to be small enough. On the other hand, according to Section III-B, with the purpose of reducing the amplitude of the limit cycle, polar plot of $G(j\omega)$ must intersect the negative real axis at a point σ located farther to the left of the point $-1/k = -1$; since in a conventional DC motor $k = 1$ is considered. This suggests that $|G(j\omega_\sigma)| \gg 1$ and this must occur at an oscillation frequency $\omega = \omega_\sigma$.

Based on the aforementioned ideas, gains k_v, α, k_d, and k_p of the control (21) are computed for the Furuta pendulum and pendubot using formulas introduced in Section IV, proceeding as follows:

1) Plot Bode diagrams of plant $G_1(s)$.
2) Propose some value for ω_σ and $|G(j\omega_\sigma)|$. A suitable value for $\omega_\sigma = 2\pi f_\sigma$ can be chosen by selecting some reasonable frequency in Hertz f_σ for oscillation of the flat output. Using this value of ω_σ and Bode diagrams plotted above, measure $|G_1(j\omega_\sigma)|$. Propose some approximate desired oscillation amplitude A_d for the flat output and using $A_d = |G_1(j\omega_\sigma)|\,A$ compute the limit cycle amplitude in the torque signal such that $A > \delta$. If this condition is not satisfied propose another larger A_d and recompute. Finally, using (26) and (27) compute $|G(j\omega_\sigma)|$.
3) Notice that (35) implies that sign of square root in (33) should be negative. However, from Figs. 2 and 3 it is also concluded that some $k_p > 0$ is necessary to ensure closed-loop stability in both Furuta pendulum and pendubot. It is clear from (33) and (35) that, in order to avoid negative values for k_p, larger values of either α or ω_σ are required. In the particular case of the Furuta pendulum, from the second degree characteristic polynomial in (28), it is concluded that a larger α is possible if the imaginary part of roots of this characteristic polynomial is larger. Moreover, a larger real part is also required to avoid bad damped responses. Thus, compute k_v and α by proposing, for transfer function in (28), poles with larger imaginary part and larger negative real part. In the case of the pendubot, compute k_v and α according to (30) and (31). If it is preferred to increase ω_σ, propose a larger value and go back to step 2).
4) Compute k_d using (37). Notice that this, (36) and (33) ensure that k_p is always real. Thus, if care was put in the previous step to select k_v and α, k_p will be positive and, hence, closed-loop stability will be ensured. Thus, if this is not the case, go back to step 3).
5) If a limit cycle appears, i.e., if F or F_P are not constants, maintain ω_σ, increase $|G(j\omega_\sigma)|$ and go back to step 3) until either limit cycle disappears or considerable mechanism vibration is observed.
6) If limit cycle does not disappear and considerable mechanism vibration is observed then increase ω_σ and choose $|G(j\omega_\sigma)|$ to be the same as in the first experiment performed with the previous ω_σ and go back to step 3).
7) If limit cycle disappears, that is, if F or F_P are constant, a successful design has been accomplished and the procedure ends.

In step 2) above, a methodology is described to select a suitable $|G(j\omega_\sigma)|$, which requires the knowledge of the parameter δ of the dead-zone nonlinearity. However, if the parameter δ is not known, step 2) can be completed using any small δ or just skip this part of step 2) to directly propose some $|G(j\omega_\sigma)|$.

Bode diagrams of the plant $G_1(j\omega)$, Furuta pendulum or pendubot, associated with step 1) are plotted in Fig. 8. Following step 2), the above procedure was initially applied to the Furuta pendulum using $\omega_\sigma = 4$ rad/s and to the pendubot using $\omega_\sigma = 10$ rad/s, which yields from Fig. 8 $|G_1(j\omega_\sigma)|_{\text{dB}} = 32.8$ dB for the Furuta pendulum and

$|G_1(j\omega_\sigma)|_{\text{dB}} = -0.232$ dB for the pendubot, i.e.,

$$|G_1(j\omega_\sigma)| = 10^{|G_1(j\omega_\sigma)|_{\text{dB}}/20} = 44.1570, \quad (41)$$
$$|G_1(j\omega_\sigma)| = 10^{|G_1(j\omega_\sigma)|_{\text{dB}}/20} = 0.9735, \quad (42)$$

respectively. Also, $|G(j\omega_\sigma)| = 4$ was initially employed in both cases.

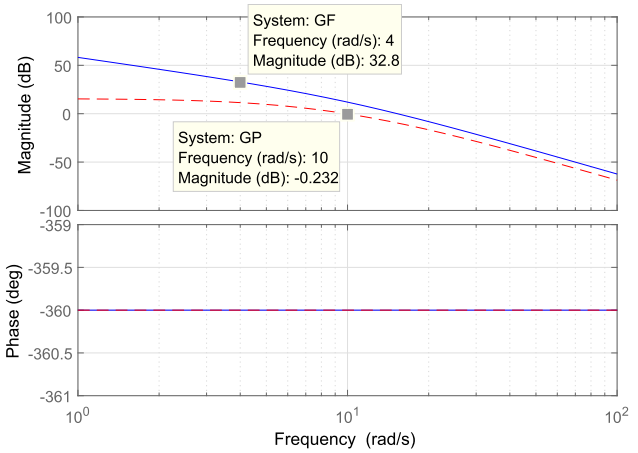

FIGURE 8. Bode diagrams of $G_1(s)$. Continuous line: Furuta pendulum. Dash line: pendubot.

In step 3), k_v and α were computed for the Furuta pendulum using the characteristic polynomial of (28), obtaining the following:

$$k_v = 0.00035, \qquad \alpha = 0.0073,$$

whereas for the pendubot they were computed using (30) and (31), founding:

$$k_v = 0.00140, \qquad \alpha = 0.0411.$$

These numerical values were used to find:

$$|G_2(j\omega_\sigma)| = \frac{4}{44.1570} = 0.0906, \quad (43)$$

and

$$|G_2(j\omega_\sigma)| = \frac{10}{0.9735} = 4.1088, \quad (44)$$

respectively.

With the numerical value in (43) and (44), (33) and (37) were computed founding the constants:

$$k_p = 0.0259, \quad k_d = 0.0056, \quad (45)$$

and

$$k_p = 0.0012, \quad k_d = 0.1400, \quad (46)$$

for the Furuta pendulum and pendubot, respectively.

As stated in step 3), sign "−" was used in (33) since this renders $k_p - \alpha\omega_\sigma^2 = -0.0906 < 0$ for Furuta pendulum and $k_p - \alpha\omega_\sigma^2 = -4.1088 < 0$ for the pendubot. Therefore, in the case of the Furuta pendulum, when using the relations in (23) the following gains for the linear state feedback controller (22) were found:

$$k_1 = -0.0238, \quad k_2 = -0.0056,$$
$$k_3 = -0.5381, \quad k_4 = -0.0321. \quad (47)$$

Similarly in the case of the pendubot, when using the relations in (24) the following gains for (22) were found:

$$k_1 = -1.2045, \quad k_2 = -0.1810,$$
$$k_3 = -1.2038, \quad k_4 = -0.0974. \quad (48)$$

Bode diagrams of the compensated systems $G(s)$ are shown in Fig. 9. There, it is corroborated that systems in open-loop have the desired phase and magnitude, that is $-180°$, and $|G(j\omega_\sigma)|_{\text{dB}} = 12$, i.e., $|G(j\omega_\sigma)| \approx 4$. This can also be clearly seen in polar plot of $G(j\omega)$ depicted in Fig. 10.

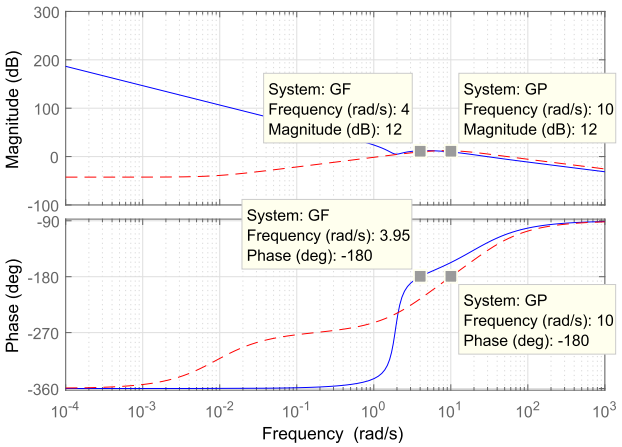

FIGURE 9. Bode diagrams of $G(s)$. Continuous line: Furuta pendulum. Dash line: pendubot.

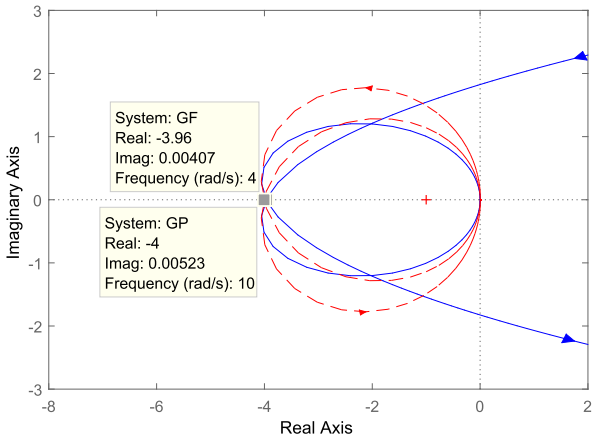

FIGURE 10. Polar plot of $G(j\omega)$. Continuous line: Furuta pendulum. Dash line: pendubot.

On the one hand, the linear state feedback control (22) with the gains in (47) was experimentally implemented to stabilize the Furuta pendulum prototype. Since (22) only stabilizes the prototype at $x_\delta = 0$ when operating close to (4), the controller reported in [43] and [44] was used to swing-up the pendulum from the initial position $\theta_1 = \pi$. Therefore, the switching

condition that obeys the controllers (22), with (47), and the one reported in [43] and [44] was determined as:

$$\begin{cases} \tau = 0.18/5 \text{ Nm} & \text{for} \quad t < 0.1 \text{ s}, \\ (22) & \text{for} \quad \sqrt{x_{\delta 3}^2 + x_{\delta 4}^2} \leq 0.3, \\ [43], [44] & \text{for} \quad \sqrt{x_{\delta 3}^2 + x_{\delta 4}^2} > 0.3. \end{cases} \tag{49}$$

where $x_{\delta 3}$ and $x_{\delta 4}$ stand as in (2).

It is important to remark that one of effects of friction on the Furuta pendulum during the swing-up stage is that pendulum may reach the inverted configuration when arm position is far from zero. Hence, if this variable is used in the above switching condition, this condition might never be satisfied. In fact, this is the behavior that has been observed in experiments and this has motivated formulation of the above switching condition.

On the other hand, (22) was also experimentally tested to stabilize the pendubot using gains in (48). In this case, the swing-up stage was carried out manually. The switching condition that obeys the controller (22), with (48), and the manual action was determined as:

$$\begin{cases} (22) & \text{for } \sqrt{x_{\delta 3}^2 + 0.1 x_{\delta 4}^2} \leq 0.5 \ \wedge \ |x_{\delta 1}| \leq 0.3, \\ \text{manual action} & \text{for } \sqrt{x_{\delta 3}^2 + 0.1 x_{\delta 4}^2} > 0.5 \ \wedge \ |x_{\delta 1}| > 0.3, \end{cases} \tag{50}$$

where $x_{\delta 1}$, $x_{\delta 3}$, and $x_{\delta 4}$ stand as in (5).

The results of the experimental implementation of (49) and (50), are shown in Fig. 11. Only the part of time where the linear controller is working is shown in this figure. In Fig. 11 it is observed that a limit cycle appears in both systems under study. For the Furuta pendulum the amplitude $A_{eF} = 0.0526$ Nm and oscillation frequency $\omega_{\sigma eF} = 1.6377$ rad/s of the limit cycle were obtained from the torque signal. Whereas, for the pendubot the amplitude $A_{eP} = 0.0605$ Nm and oscillation frequency $\omega_{\sigma eP} = 2.2737$ rad/s of the limit cycle were obtained also from the torque signal. Note that θ_1 remains close to 2π. Recall that the linear approximate model in (1) with (2) is also valid for $\overline{\theta}_1 = \pm 2\pi$.

All gains that were computed and experimentally tested are shown in Tables 2 and 3. These tables also include the amplitude and oscillation frequency of the limit cycle measured from each experiment. In Table 2, which refers to the Furuta pendulum, amplitude and oscillation frequency of the limit cycle are denoted as A_{eF} and $\omega_{\sigma eF}$, respectively. Whereas in Table 3, which refers to the pendubot, amplitude and oscillation frequency of the limit cycle are denoted as A_{eP} and $\omega_{\sigma eP}$, respectively. The experiment where the limit cycle was completely eliminated is located, for the Furuta pendulum, at $|G(j\omega_\sigma)| = 17$ and $\omega_\sigma = 8$ rad/s in Table 2 and, for the pendubot, at $|G(j\omega_\sigma)| = 25$ and $\omega_\sigma = 14$ rad/s in Table 3. In order to give an idea of the evolution of the Furuta pendulum and pendubot experiments from the one presented in Fig. 11, Fig. 12 shows the results when $|G(j\omega_\sigma)| = 11$ and $\omega_\sigma = 6$ rad/s are considered for the Furuta pendulum and when $|G(j\omega_\sigma)| = 12$ and $\omega_\sigma = 12$ rad/s are taken into account for the pendubot, in which the amplitude and oscillation frequency of the limit cycle are $A_{eF} = 0.0221$ Nm and $\omega_{\sigma eF} = 0.8304$ rad/s, respectively, for the Furuta pendulum, and $A_{eP} = 0.0365$ Nm and $\omega_{\sigma eP} = 1.9635$ rad/s, respectively, for the pendubot. Note that in both systems the amplitude of the limit cycle in Fig. 12 is smaller than the amplitude of limit cycle in Fig. 11 and $|G(j\omega_\sigma)| \gg 1$ is satisfied, which is in accordance with Sections III-B and V-A. Whereas, the result where the limit cycle is completely eliminated is presented in Fig. 13. It is important to say that for the Furuta pendulum the limit cycle is partially eliminated when using set of gains related to $|G(j\omega_\sigma)| = 13$ and $\omega_\sigma = 8$ rad/s, that is, occasionally some oscillations appear. This is the reason of why $A_{eF} \leq \delta$ is reported in Table 2 when $|G(j\omega_\sigma)| = 13$ and $\omega_\sigma = 8$ rad/s. The gains associated with the experimental results in Figs. 11, 12, and 13 (when limit cycle is completely eliminated) have been highlighted in Tables 2 and 3. Furthermore, Fig. 14 shows how the amplitude of the limit cycle changes until vanishes during the experimental procedure as $|G(j\omega_\sigma)|$ and ω_σ are larger in both prototypes. In such a figure it is clear that $A_{eF} < \delta = 0.00817$ and $A_{eP} < \delta = 0.0232$. Also, in Fig. 14 it can be seen that amplitudes A_{eF} and A_{eP} of limit cycles of the Furuta pendulum and pendubot, respectively, are smaller for a given $|G(j\omega_\sigma)|$ if ω_σ is chosen to be larger. According to conjecture in Section V-A, this is useful to eliminate limit cycle because a too large value of $|G(j\omega_\sigma)|$ may result in excessive vibration, due to noise, instead of limit cycle elimination.

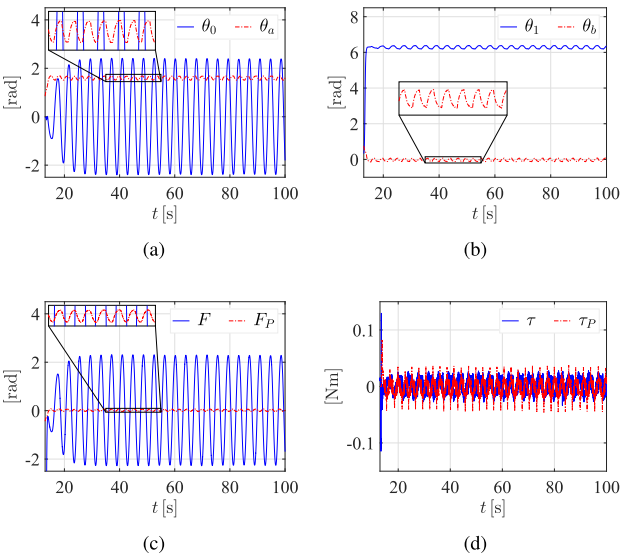

FIGURE 11. Experimental results when considering (47) for the Furuta pendulum and (48) for the pendubot.

In order to verify robustness of the proposed control scheme, an additional experiment was performed which consisted in two parts. First, when $t \leq 40$ [s] the linear state feedback controller (22) was implemented using the best gains obtained by the authors via the Matlab acker() function,

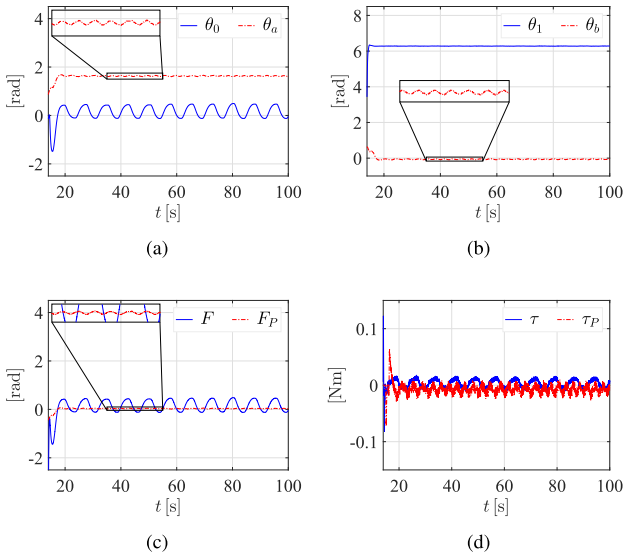

FIGURE 12. Experimental results when considering $|G(j\omega_\sigma)| = 11$ and $\omega_\sigma = 6$ rad/s for the Furuta pendulum as well as $|G(j\omega_\sigma)| = 12$ and $\omega_\sigma = 12$ rad/s for the pendubot.

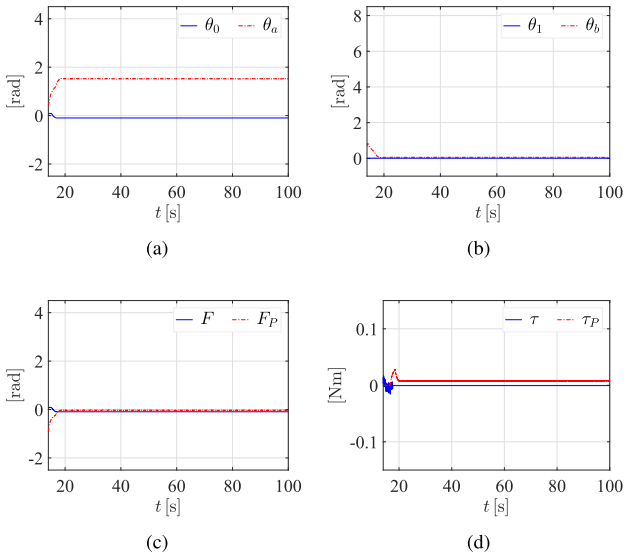

FIGURE 13. Experimental results when considering for the Furuta pendulum $|G(j\omega_\sigma)| = 17$ and $\omega_\sigma = 8$ rad/s and for the pendubot $|G(j\omega_\sigma)| = 25$ and $\omega_\sigma = 14$ rad/s.

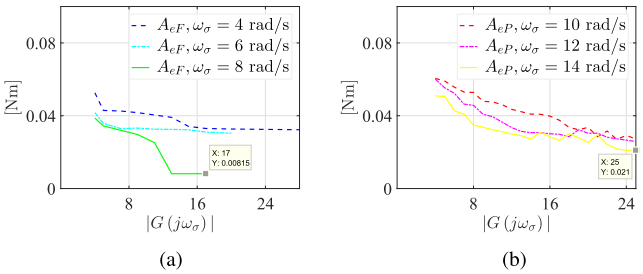

FIGURE 14. Evolution of the limit cycle amplitude during experimental procedure.

that is, the following gains for the Furuta pendulum:

$$k_1 = -0.1301, \quad k_2 = -0.1041,$$
$$k_3 = -1.8905, \quad k_4 = -0.2170, \tag{51}$$

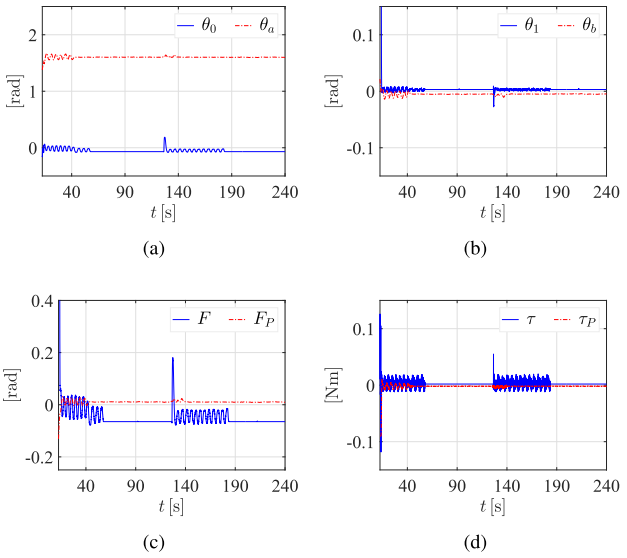

FIGURE 15. Experimental results with disturbances.

and the following gains for the pendubot:

$$k_1 = -3.9597, \quad k_2 = -0.6357,$$
$$k_3 = -3.6777, \quad k_4 = -0.3316, \tag{52}$$

and with which a limit cycle exist in both prototypes. Then, when $t > 40$ [s] the gains of (22) were switched to the ones that eliminate the limit cycle, that is, gains at bottom of the third column of Tables 2 and 3 for the Furuta pendulum and pendubot, respectively. Second, once the limit cycle was eliminated, the prototypes were kicked intentionally just to perturb the systems. The corresponding experimental results are shown in Fig. 15. There, it can be seen that in the Furuta pendulum the limit cycle does not disappear immediately when switching the gains (51) to the ones that eliminate it, but it does after a short interval of time. Then, it is observed that the effect of one kick in the pendulum at $t \approx 126.5$ [s] is well countered by the controller, since limit cycle disappears again, not immediately but after a few seconds elapsed. With regards to the pendubot, in Fig. 15 it is shown that the limit cycle vanishes almost immediately when switching the gains (52) to the ones that eliminate it. The same happen when *bar B* was kicked once. Thus, with the intention of making more visible the disturbance in the pendubot, *bar B* was kicked consecutively in three times, starting the first kick at $t \approx 125$ [s]. From the results in Fig. 15, it can be concluded that the controller is successful against disturbances and, in consequence, robust to eliminate limit cycles in both inverted pendulums under study.

D. OBSERVATIONS FROM EXPERIMENTS

First important observation to make is that maximum values of $|G(j\omega_\sigma)|$ for each ω_σ, allowed by the Furuta pendulum and pedubot prototypes to perform experiments in closed-loop, appear at the bottom of each column in Tables 2 and 3,

TABLE 2. Computed gains of controls (21) and (22) for the Furuta pendulum.

$\lvert G(j\omega_\sigma)\rvert$	ω_σ		
	$4\ \frac{\text{rad}}{\text{s}}$	$6\ \frac{\text{rad}}{\text{s}}$	$8\ \frac{\text{rad}}{\text{s}}$
4	$k_v = 0.00035,\ \alpha = 0.0073,$ $k_d = 0.0056,\ k_p = 0.0259.$	$k_v = 0.00035,\ \alpha = 0.0073,$ $k_d = 0.0126,\ k_p = 0.0126.$	$k_v = 0.0004375,\ \alpha = 0.0091,$ $k_d = 0.0280,\ k_p = 0.0671.$
	$k_1 = -0.0238,\ k_2 = -0.0056,$ $k_3 = -0.5381,\ k_4 = -0.0321.$	$k_1 = -0.0126,\ k_2 = -0.0126,$ $k_3 = -0.5226,\ k_4 = -0.0418.$	$k_1 = -0.0671,\ k_2 = -0.0280,$ $k_3 = -0.7247,\ k_4 = -0.0693.$
	$A_{eF} = 0.0526$ Nm, $\omega_{\sigma e} = 1.6377\ \frac{\text{rad}}{\text{s}}$	$A_{eF} = 0.0417$ Nm, $\omega_{\sigma e} = 0.6405\ \frac{\text{rad}}{\text{s}}$	$A_{eF} = 0.0387$ Nm, $\omega_{\sigma e} = 1.6323\ \frac{\text{rad}}{\text{s}}$
5	$k_v = 0.0004375,\ \alpha = 0.0091,$ $k_d = 0.0070,\ k_p = 0.0297.$	$k_v = 0.0004375,\ \alpha = 0.0091,$ $k_d = 0.0158,\ k_p = 0.0157.$	$k_v = 0.000525,\ \alpha = 0.0109,$ $k_d = 0.0336,\ k_p = 0.0548.$
	$k_1 = -0.0297,\ k_2 = -0.0070,$ $k_3 = -0.6727,\ k_4 = -0.0401.$	$k_1 = -0.0157,\ k_2 = -0.0158,$ $k_3 = -0.6532,\ k_4 = -0.0523.$	$k_1 = -0.0548,\ k_2 = -0.0336,$ $k_3 = -0.8338,\ k_4 = -0.0832.$
	$A_{eF} = 0.0429$ Nm, $\omega_{\sigma e} = 1.5982\ \frac{\text{rad}}{\text{s}}$	$A_{eF} = 0.0358$ Nm, $\omega_{\sigma e} = 0.6467\ \frac{\text{rad}}{\text{s}}$	$A_{eF} = 0.0344$ Nm, $\omega_{\sigma e} = 0.9973\ \frac{\text{rad}}{\text{s}}$
9	$k_v = 0.0006125,\ \alpha = 0.0127,$ $k_d = 0.0098,\ k_p = 0.0416.$	$k_v = 0.0006125,\ \alpha = 0.0127,$ $k_d = 0.0221,\ k_p = 0.0220.$	$k_v = 0.0007,\ \alpha = 0.0146,$ $k_d = 0.0448,\ k_p = 0.0301.$
	$k_1 = -0.0535,\ k_2 = -0.0126,$ $k_3 = -1.2108,\ k_4 = -0.0722.$	$k_1 = -0.0283,\ k_2 = -0.0283,$ $k_3 = -1.1758,\ k_4 = -0.0941.$	$k_1 = -0.0054,\ k_2 = -0.0560,$ $k_3 = -1.2701,\ k_4 = -0.1386.$
	$A_{eF} = 0.0417$ Nm, $\omega_{\sigma e} = 1.5676\ \frac{\text{rad}}{\text{s}}$	$A_{eF} = 0.0332$ Nm, $\omega_{\sigma e} = 0.7847\ \frac{\text{rad}}{\text{s}}$	$A_{eF} = 0.0297$ Nm, $\omega_{\sigma e} = 1.4090\ \frac{\text{rad}}{\text{s}}$
11	$k_v = 0.0009625,\ \alpha = 0.0200,$ $k_d = 0.0154,\ k_p = 0.0654.$	$k_v = 0.0009625,\ \alpha = 0.0200,$ $k_d = 0.0347,\ k_p = -0.0347.$	$k_v = 0.0011,\ \alpha = 0.0237,$ $k_d = 0.0728,\ k_p = 0.0642.$
	$k_1 = -0.0654,\ k_2 = -0.0154,$ $k_3 = -1.4799,\ k_4 = -0.0882.$	$k_1 = -0.0346,\ k_2 = -0.0283,$ $k_3 = -1.4371,\ k_4 = -0.1150.$	$k_1 = -0.0642,\ k_2 = -0.0728,$ $k_3 = -1.7307,\ k_4 = -0.1802.$
	$A_{eF} = 0.0404$ Nm, $\omega_{\sigma e} = 1.5506\ \frac{\text{rad}}{\text{s}}$	$A_{eF} = 0.0326$ Nm, $\omega_{\sigma e} = 0.8208\ \frac{\text{rad}}{\text{s}}$	$A_{eF} = 0.0252$ Nm, $\omega_{\sigma e} = 0.8394\ \frac{\text{rad}}{\text{s}}$
13	$k_v = 0.0011,\ \alpha = 0.0237,$ $k_d = 0.0182,\ k_p = 0.0773.$	$k_v = 0.0011,\ \alpha = 0.0237,$ $k_d = 0.0409,\ k_p = 0.0409.$	$k_v = 0.0013,\ \alpha = 0.0273,$ $k_d = 0.0840,\ k_p = 0.0335.$
	$k_1 = -0.0773,\ k_2 = -0.0182,$ $k_3 = -1.7490,\ k_4 = -0.1042.$	$k_1 = -0.0409,\ k_2 = -0.0409,$ $k_3 = -1.6984,\ k_4 = -0.1359.$	$k_1 = -0.0335,\ k_2 = -0.0840,$ $k_3 = -1.9406,\ k_4 = -0.2079.$
	$A_{eF} = 0.0391$ Nm, $\omega_{\sigma e} = 1.5594\ \frac{\text{rad}}{\text{s}}$	$A_{eF} = 0.0325$ Nm, $\omega_{\sigma e} = 0.7507\ \frac{\text{rad}}{\text{s}}$	$A_{eF} \leq \delta$ Nm, $\omega_{\sigma e} = 0\ \frac{\text{rad}}{\text{s}}$
17	$k_v = 0.0015,\ \alpha = 0.0309,$ $k_d = 0.0238,\ k_p = 0.1011.$	$k_v = 0.0015,\ \alpha = 0.0309,$ $k_d = 0.0535,\ k_p = 0.0535.$	$k_v = 0.0017,\ \alpha = 0.0364,$ $k_d = 0.1120,\ k_p = 0.0886.$
	$k_1 = -0.1011,\ k_2 = -0.0238,$ $k_3 = -2.2871,\ k_4 = -0.1363.$	$k_1 = -0.0535,\ k_2 = -0.0535,$ $k_3 = -2.2209,\ k_4 = -0.1777.$	$k_1 = -0.0886,\ k_2 = -0.1120,$ $k_3 = -2.6485,\ k_4 = -0.2772.$
	$A_{eF} = 0.0330$ Nm, $\omega_{\sigma e} = 1.4857\ \frac{\text{rad}}{\text{s}}$	$A_{eF} = 0.0310$ Nm, $\omega_{\sigma e} = 0.7819\ \frac{\text{rad}}{\text{s}}$	$A_{eF} \leq \delta$ Nm, $\omega_{\sigma e} = 0\ \frac{\text{rad}}{\text{s}}$
20	$k_v = 0.0017,\ \alpha = 0.0364,$ $k_d = 0.0280,\ k_p = 0.1189.$	$k_v = 0.0017,\ \alpha = 0.0364,$ $k_d = 0.0630,\ k_p = 0.0629.$	
	$k_1 = -0.1189,\ k_2 = -0.0280,$ $k_3 = -2.6907,\ k_4 = -0.1604.$	$k_1 = -0.0629,\ k_2 = -0.0630,$ $k_3 = -2.6129,\ k_4 = -0.2090.$	
	$A_{eF} = 0.0327$ Nm, $\omega_{\sigma e} = 1.5396\ \frac{\text{rad}}{\text{s}}$	$A_{eF} = 0.0304$ Nm, $\omega_{\sigma e} = 0.8004\ \frac{\text{rad}}{\text{s}}$	
28	$k_v = 0.0024,\ \alpha = 0.0510,$ $k_d = 0.0392,\ k_p = 0.1665.$		
	$k_1 = -0.1665,\ k_2 = -0.0392,$ $k_3 = -3.6891,\ k_4 = -0.2926.$		
	$A_{eF} = 0.0323$ Nm, $\omega_{\sigma e} = 1.5323\ \frac{\text{rad}}{\text{s}}$		

respectively. After that values, the prototypes presented notable vibration. Thus, from Table 2, i.e., for the Furuta pendulum, it can be concluded that lower frequencies allow larger magnitudes of $G(j\omega)$ and that at larger frequencies magnitude of $G(j\omega)$ must be decreased to avoid excessive vibration in the closed-loop system and to approach to the limit cycle elimination. In contrast with Table 2, in Table 3, which refers to the pendubot, same magnitud of $G(j\omega_\sigma)$ is reached for all ω_σ.

Second observation is that experimental results corroborate conjecture in Section V-A, i.e., that limit cycle is eliminated as selecting gains of controller such that polar plot of $G(j\omega)$ crosses the negative real axis at a point located farther to the left. Moreover, an additional observation from the

TABLE 3. Computed gains of controls (21) and (22) for the pendubot.

$\lvert G(j\omega_\sigma)\rvert$	ω_σ		
	10 $\frac{\text{rad}}{\text{s}}$	12 $\frac{\text{rad}}{\text{s}}$	14 $\frac{\text{rad}}{\text{s}}$
4	$k_v = 0.0014$, $\alpha = 0.0411$, $k_d = 0.1400$, $k_p = 0.0012$.	$k_v = 0.001$, $\alpha = 0.0434$, $k_d = 0.1440$, $k_p = 0.0042$.	$k_v = 0.001$, $\alpha = 0.049$, $k_d = 0.1960$, $k_p = 0.2594$.
	$k_1 = -1.2045$, $k_2 = -0.1810$, $k_3 = -1.2038$, $k_4 = -0.0974$.	$k_1 = -1.2748$, $k_2 = -0.1733$, $k_3 = -1.2723$, $k_4 = -0.0873$.	$k_1 = -1.6940$, $k_2 = -0.2253$, $k_3 = -1.5392$, $k_4 = -0.1083$.
	$A_{eP} = 0.0605$ Nm, $\omega_{\sigma eP} = 2.2737$ $\frac{\text{rad}}{\text{s}}$	$A_{eP} = 0.0601$ Nm, $\omega_{\sigma eP} = 2.0039$ $\frac{\text{rad}}{\text{s}}$	$A_{eP} = 0.0509$ Nm, $\omega_{\sigma eP} = 3.1918$ $\frac{\text{rad}}{\text{s}}$
7	$k_v = 0.0019$, $\alpha = 0.072$, $k_d = 0.1900$, $k_p = 0.0097$.	$k_v = 0.0015$, $\alpha = 0.076$, $k_d = 0.2160$, $k_p = 0.0146$.	$k_v = 0.0014$, $\alpha = 0.084$, $k_d = 0.2744$, $k_p = 0.1110$.
	$k_1 = -2.1176$, $k_2 = -0.2456$, $k_3 = -2.1119$, $k_4 = -0.1322$.	$k_1 = -0.2599$, $k_2 = -0.2599$, $k_3 = -2.2309$, $k_4 = -0.1310$.	$k_1 = -2.5702$, $k_2 = -0.3154$, $k_3 = -2.5040$, $k_4 = -0.1516$.
	$A_{eP} = 0.0530$ Nm, $\omega_{\sigma eP} = 1.8125$ $\frac{\text{rad}}{\text{s}}$	$A_{eP} = 0.0464$ Nm, $\omega_{\sigma eP} = 1.5272$ $\frac{\text{rad}}{\text{s}}$	$A_{eP} = 0.0408$ Nm, $\omega_{\sigma eP} = 2.0790$ $\frac{\text{rad}}{\text{s}}$
10	$k_v = 0.0023$, $\alpha = 0.103$, $k_d = 0.2300$, $k_p = 0.0281$.	$k_v = 0.0021$, $\alpha = 0.109$, $k_d = 0.3024$, $k_p = 0.0825$.	$k_v = 0.0019$, $\alpha = 0.12$, $k_d = 0.3724$, $k_p = 0.1585$.
	$k_1 = -3.0437$, $k_2 = -0.2973$, $k_3 = -3.0269$, $k_4 = -0.1601$.	$k_1 = -3.2737$, $k_2 = -0.3639$, $k_3 = -3.2245$, $k_4 = -0.1834$.	$k_1 = -3.6718$, $k_2 = -0.4280$, $k_3 = -3.5772$, $k_4 = -0.2057$.
	$A_{eP} = 0.0476$ Nm, $\omega_{\sigma eP} = 1.4226$ $\frac{\text{rad}}{\text{s}}$	$A_{eP} = 0.0335$ Nm, $\omega_{\sigma eP} = 1.6698$ $\frac{\text{rad}}{\text{s}}$	$A_{eP} = 0.0323$ Nm, $\omega_{\sigma eP} = 2.6050$ $\frac{\text{rad}}{\text{s}}$
12	$k_v = 0.0026$, $\alpha = 0.124$, $k_d = 0.2600$, $k_p = 0.0737$.	$k_v = 0.0026$, $\alpha = 0.131$, $k_d = 0.3744$, $k_p = 0.1278$.	$k_v = 0.0022$, $\alpha = 0.144$, $k_d = 0.4312$, $k_p = 0.1902$.
	$k_1 = -3.7041$, $k_2 = -0.3361$, $k_3 = -3.6601$, $k_4 = -0.1809$.	$k_1 = -3.9631$, $k_2 = -0.4505$, $k_3 = -3.8868$, $k_4 = -0.2270$.	$k_1 = -4.4061$;, $k_2 = -4.4061$;, $k_3 = -4.2926$, $k_4 = -0.2382$.
	$A_{eP} = 0.0435$ Nm, $\omega_{\sigma eP} = 1.6046$ $\frac{\text{rad}}{\text{s}}$	$A_{eP} = 0.0302$ Nm, $\omega_{\sigma eP} = 1.9778$ $\frac{\text{rad}}{\text{s}}$	$A_{eP} = 0.0300$ Nm, $\omega_{\sigma eP} = 1.8990$ $\frac{\text{rad}}{\text{s}}$
15	$k_v = 0.0029$, $\alpha = 0.155$, $k_d = 0.2900$, $k_p = 0.0922$.	$k_v = 0.003$, $\alpha = 0.164$, $k_d = 0.1958$, $k_p = 0.4320$.	$k_v = 0.0026$, $\alpha = 0.18$, $k_d = 0.5096$, $k_p = 0.2378$.
	$k_1 = -4.6301$, $k_2 = -0.3749$, $k_3 = -4.5751$, $k_4 = 0.2018$.	$k_1 = -4.9972$, $k_2 = -0.5198$, $k_3 = -4.8804$, $k_4 = -0.2620$.	$k_1 = -5.5077$, $k_2 = 0.5857$, $k_3 = 5.3657$, $k_4 = 0.2815$.
	$A_{eP} = 0.0408$ Nm, $\omega_{\sigma eP} = 1.2036$ $\frac{\text{rad}}{\text{s}}$	$A_{eP} = 0.0307$ Nm, $\omega_{\sigma eP} = 1.2487$ $\frac{\text{rad}}{\text{s}}$	$A_{eP} = 0.0309$ Nm, $\omega_{\sigma eP} = 2.3015$ $\frac{\text{rad}}{\text{s}}$
18	$k_v = 0.0032$, $\alpha = 0.185$, $k_d = 0.3200$, $k_p = 0.0106$.	$k_v = 0.0033$, $\alpha = 0.197$, $k_d = 0.4752$, $k_p = 0.2637$.	$k_v = 0.0031$, $\alpha = 0.216$ $k_d = 0.6076$, $k_p = 0.2854$.
	$k_1 = -5.4269$, $k_2 = -0.4137$, $k_3 = -5.4205$, $k_4 = -0.2227$.	$k_1 = -6.0313$, $k_2 = -0.5718$, $k_3 = -5.8739$, $k_4 = -0.2882$.	$k_1 = -6.6092$, $k_2 = -0.6984$, $k_3 = -6.4389$, $k_4 = -0.3357$.
	$A_{eP} = 0.0336$ Nm, $\omega_{\sigma eP} = 1.8219$ $\frac{\text{rad}}{\text{s}}$	$A_{eP} = 0.0285$ Nm, $\omega_{\sigma eP} = 1.4550$ $\frac{\text{rad}}{\text{s}}$	$A_{eP} = 0.0301$ Nm, $\omega_{\sigma eP} = 3.5677$ $\frac{\text{rad}}{\text{s}}$
21	$k_v = 0.0035$, $\alpha = 0.216$, $k_d = 0.3500$, $k_p = 0.0290$.	$k_v = 0.0036$, $\alpha = 0.229$, $k_d = 0.5184$, $k_p = 0.1877$.	$k_v = 0.0035$, $\alpha = 0.252$, $k_d = 0.6860$, $k_p = 0.3329$.
	$k_1 = -6.3529$, $k_2 = -0.4525$, $k_3 = 6.3356$, $k_4 = 0.2436$.	$k_1 = -6.8921$, $k_2 = -0.6238$, $k_3 = -6.7801$, $k_4 = -0.3144$.	$k_1 = -7.7107$, $k_2 = -0.7885$, $k_3 = -7.5120$, $k_4 = -0.3790$.
	$A_{eP} = 0.0285$ Nm, $\omega_{\sigma eP} = 1.3451$ $\frac{\text{rad}}{\text{s}}$	$A_{eP} = 0.0304$ Nm, $\omega_{\sigma eP} = 2.2820$ $\frac{\text{rad}}{\text{s}}$	$A_{eP} = 0.0296$ Nm, $\omega_{\sigma eP} = 1.4981$ $\frac{\text{rad}}{\text{s}}$
25	$k_v = 0.0039$, $\alpha = 0.257$, $k_d = 0.3900$, $k_p = 0.0203$.	$k_v = 0.004$, $\alpha = 0.272$, $k_d = 0.5760$, $k_p = 0.1343$.	$k_v = 0.0039$, $\alpha = 0.299$, $k_d = 0.7644$, $k_p = 0.2003$.
	$k_1 = -7.5445$, $k_2 = -0.5042$, $k_3 = -7.5324$, $k_4 = -0.2714$.	$k_1 = -8.0976$, $k_2 = -0.6931$, $k_3 = -8.0175$, $k_4 = -0.3493$.	$k_1 = -8.9542$, $k_2 = -0.8786$, $k_3 = -8.8346$, $k_4 = -0.4223$.
	$A_{eP} = 0.0272$ Nm, $\omega_{\sigma eP} = 1.4470$ $\frac{\text{rad}}{\text{s}}$	$A_{eP} = 0.0258$ Nm, $\omega_{\sigma eP} = 1.7018$ $\frac{\text{rad}}{\text{s}}$	$A_{eP} \leq \delta$ Nm, $\omega_{\sigma e} = 0$ $\frac{\text{rad}}{\text{s}}$

experiments is that limit cycle elimination is accomplished as frequency ω_σ, where polar plot of $G(j\omega)$ crosses the negative real axis, is chosen larger.

It is important to stress that in [41] it is stated that, because of the approximate nature of the describing function method, results are not very accurate some times, i.e., *a)* the predicted amplitude and frequency might not be accurate, *b)* a predicted limit cycle might actually not exist, or *c)* an existing limit cycle is not predicted. Moreover, the first kind of inaccuracy, i.e., *a)*, is quite common. Furthermore, dead-zone is an idealization of the nonlinear phenomenon that is actually present in the practical plant. This explains differences between experimental and desired frequencies.

E. ADVANTAGES OF THE PROPOSED CONTROL DESIGN METHOD

In this section, a brief comparison between the stabilizing control design method presented in this paper to

eliminate limit cycles and that introduced in [32] is presented.

- First. The design method in [32] is based on the time response approach, i.e., root locus, whereas in the present paper the frequency response approach is employed.
- Second. Notice that, according to the describing function method, conjecture introduced in Section V-A in the present paper, and experiments in Section V-C, two parameters are found to be important for limit cycle elimination: magnitude $|G(j\omega_\sigma)|$ and frequency ω_σ. The fact that both of these parameters are naturally defined in the open-loop system entails that frequency response is instrumental to obtain precise formulas, such as those in (33) and (37), useful to compute the control gains k_p and k_d in the present paper. On the other hand, although parameters $|G(j\omega_\sigma)|$ and ω_σ are also equally important for limit cycle elimination in [32], precise formulas to compute control gains satisfying these parameters do not exist. In order to compute control gains k_p and k_d in that paper, intuitive ideas must be employed to, by means of a guess-based procedure, assign an open loop zero which, it is guessed, will approximately modify the resulting $|G(j\omega_\sigma)|$ and ω_σ in the expected direction.
- Third. In the present paper k_v and α are computed by assigning poles of transfer function in (28) and (29) farther to the left with a larger imaginary part. Reasons for this are precisely explained from (33) because use of this expression must ensure that a positive k_p will be obtained, i.e., to ensure closed-loop stability. Notice that (33) gives a precise condition that α must satisfy. Thus, poles may be proposed iteratively until such a condition is satisfied. See item 3) in procedure introduced in Section V-C. On the other hand, in [32], k_v and β must also be computed by assigning poles of a second order transfer function similar to that in (28) in the present paper. Moreover, these poles also must be placed farther to the left with a larger imaginary part. However, reasons for this pole assignment is rather intuitive instead of precise. Since this transfer function is obtained by closing two internal loops (see Fig. 2, for instance), root locus-based arguments in [32] make the designer just to guess that such a pole assignment could also render possible to assign farther to the left the closed-loop poles. This is an imprecise procedure since the closed-loop poles have to be assigned by means of the external loop, i.e., to be performed in the next step of the design procedure. Moreover, this assignment rule for the closed-loop poles is concluded by guessing that faster closed-loop poles will result in larger values for $|G(j\omega_\sigma)|$ and ω_σ. Although this is a correct guess, however there is no manner to ensure that precise values for this parameters will be assigned. This is also stated in the previous paragraph.
- Four. When procedure reported in [32] was applied to the Furuta pendulum shown in Fig. 6 in the present paper, successful results were not obtained, that is, limit cycle was not eliminated. This is illustrated in Fig. 16 where some results are presented using the following controller gains:

$$\begin{aligned} k_1 &= -3.8029, \quad k_2 = -0.9120, \\ k_3 &= -8.4526, \quad k_4 = -1.4420. \end{aligned} \tag{53}$$

which were computed using the tuning procedure in [32]. This is the limit cycle with the smallest amplitude that was possible to accomplish.
The controller in [32] cannot be applied to the pendubot, this is the reason of why experimental results of the pendubot in closed-loop with controller in [32] are not presented.

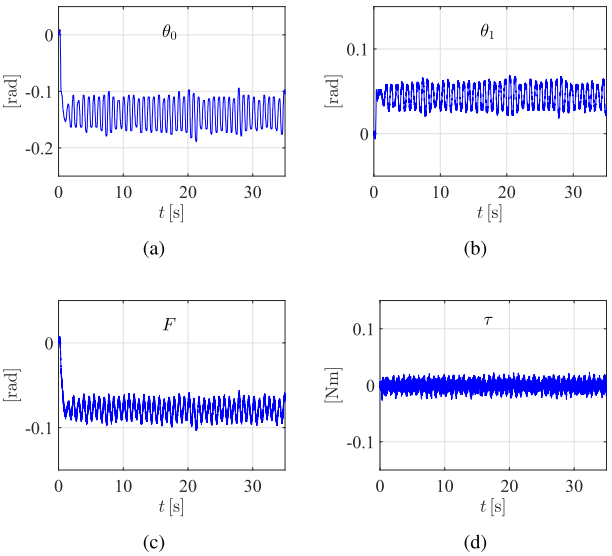

FIGURE 16. Better experimental results obtained when following [32] for Furuta pendulum in Fig. 6.

In contrast with the results in Fig. 16, an experiment was performed to test the controller and tuning procedure proposed in this paper when using the Furuta pendulum prototype reported in [32]. The reader is referred to that paper for information on the numerical values of parameters of that experimental prototype. Two sets of controller gains were tested. The first one was computed by proposing $\omega_\sigma = 7.2$ [rad/s], $|G(j\omega_\sigma)| = 3.7792$, and the complex conjugate poles $-15 \pm 17j$ for transfer function in (28). This results in:

$$\begin{aligned} k_1 &= -0.0202, \quad k_2 = -0.0128, \\ k_3 &= -0.3410, \quad k_4 = -0.0315. \end{aligned} \tag{54}$$

The second set of gains was computed by proposing $\omega_\sigma = 11.8$ [rad/s], $|G(j\omega_\sigma)| = 8.87$, and the complex conjugate poles $-24.3 \pm 37.5j$ for transfer function in (28), resulting the following:

$$\begin{aligned} k_1 &= -0.0302, \quad k_2 = -0.0550, \\ k_3 &= -1.1263, \quad k_4 = -0.0940. \end{aligned} \tag{55}$$

In Fig. 17 the experimental results are presented when using the controller gains in (55) for $t < 35$ [s] and $t > 55$ [s] and the controller gains in (54) for 35 [s] $\leq t \leq$ 55 [s]. Notice that the limit cycle disappears when controller gains in (55) are employed, which are computed by using larger values for both ω_σ and $|G(j\omega_\sigma)|$. Thus, these results are in agreement with the results obtained in the present paper for the Furuta pendulum in Fig. 6.

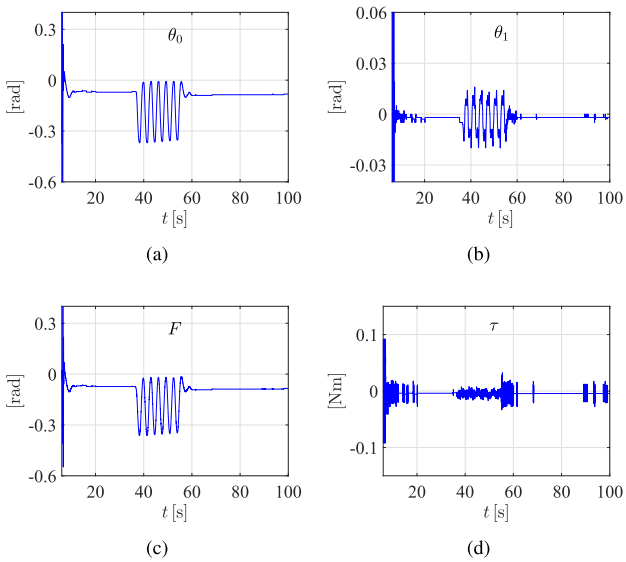

FIGURE 17. Experimental results of the Furuta pendulum in [32] when using (54) and (55) obtained following procedure described in this paper.

From Figs. 16 and 17, it can be concluded the following: it is difficult to obtain successful results when applying controller and tuning procedure described in [32] to eliminate limit cycle in other Furuta pendulums due to the procedure nature based on a guess. Whereas controller and tuning procedure reported in this paper to eliminate limit cycle is easy to repeat in other Furuta pendulums. Until here, a performance comparison between the controller and tuning procedure herein reported against the controller and tuning procedure in [32] has been carried out when using different prototypes of the Furuta pendulum.

Now, since behavior of the controller and procedure here proposed to eliminate limit cycle in the Furuta pendulum prototype of [32] is known as successful (see Fig. 17). It is important to compare the robustness of the controller herein reported with that reported in [32], this in the sense of limit cycle elimination. Hence, another experiment in the Furuta pendulum of [32], similar to that shown in Fig. 17, was performed using two sets of gains reported in [32, Table 4], that is:

$$\begin{aligned} k_1 &= -0.0415, \quad k_2 = -0.0415, \\ k_3 &= -0.5189, \quad k_4 = -0.0728, \end{aligned} \tag{56}$$

and

$$\begin{aligned} k_1 &= -0.0118, \quad k_2 = -0.0118, \\ k_3 &= -0.2742, \quad k_4 = -0.0298, \end{aligned} \tag{57}$$

The procedure to obtain these gains is explained in [32]. We stress that controller gains in (56) are reported in [32] to eliminate the limit cycle whereas controller gains in (57) are reported not to eliminate the limit cycle. (56) was used for $t < 30$ [s] and $t > 50$ [s] whereas (57) was employed for 30 [s] $\leq t \leq 50$ [s]. Fig. 18 shows the corresponding experimental results, where there is not any important difference between the performance achieved in Fig. 17, that is, with the tuning procedure introduced in the present paper.

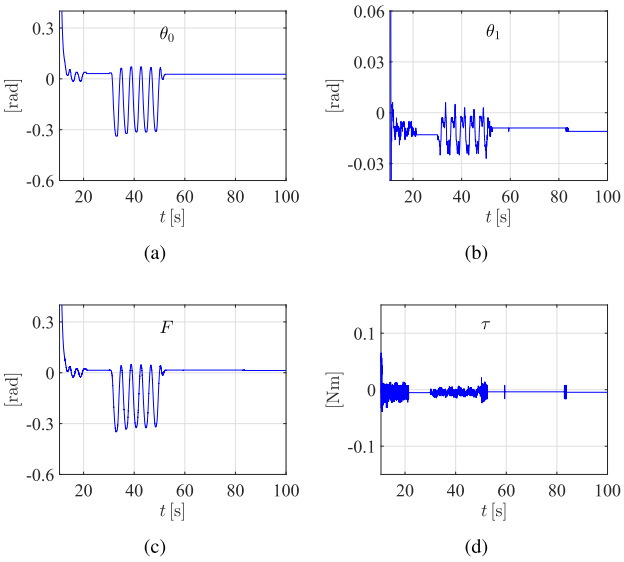

FIGURE 18. Experimental results of the Furuta pendulum in [32] when using (56) and (57) obtained following procedure described in [32].

- Lastly, it must be stressed that the proposed control scheme is not based on friction compensation techniques, which have the following disadvantages: i) most compensation terms are complex and require numerical values of frictional parameters [30], ii) undercompensation leads to steady-state error and overcompensation may induce limit cycles [20], [45]. Hence, methodology in the present paper is simple and effective for the elimination of limit cycles.

Drawbacks described above of method in [32] and friction compensation techniques have been the main motivations for the present paper.

VI. CONCLUSION

In this paper we have presented a control scheme for the stabilization of two inverted pendulum, that is, Furuta pendulum and pendubot. Such a control scheme allows eliminating the limit cycle due to the effect of a dead-zone nonlinearity induced by static friction at the motor shaft of the systems.

The proposed control exploits the differential flatness property of the system to translate a linear state feedback control design into a design based on the classical frequency domain. As the result of a describing function-based analysis we have established, as a conjecture, that controller design must be performed such that the limit cycle amplitude is rendered small enough. Successful experimental results have corroborated correctness of such a conjecture and support the effectiveness of the proposed control scheme to eliminate limit cycles. Also, robustness of the control to eliminate the limit cycle in presence of disturbances has been demonstrated. A new information resulting from experiments is that the limit cycle oscillation frequency must be chosen to be large enough in order to avoid limit cycles. Differences and advantages of this control design with respect to the one reported in [32] have also been remarked. Main advantage of this control design is the application of control theory in such a simplified fashion, rendering a method straightforward for practical application. This in comparison with control methodologies based on friction compensation. Thus, importance of this paper lays on that it could be useful for a wide acceptation of control methods in practice.

Future work contemplates application of the proposed control scheme to eliminate limit cycle in other inverted pendulums.

REFERENCES

[1] M. Ryalat and D. S. Laila, "A simplified IDA-PBC design for underactuated mechanical systems with applications," *Eur. J. Control*, vol. 27, pp. 1–16, Jan. 2016.

[2] Q. Khan, R. Akmeliawati, A. I. Bhatti, and M. A. Khan, "Robust stabilization of underactuated nonlinear systems: A fast terminal sliding mode approach," *ISA Trans.*, vol. 66, pp. 241–248, Jan. 2017.

[3] G. He, R. Chen, and Y. Zhang, "Globally stabilizing a class of underactuated mechanical systems on the basis of finite-time stabilizing observer," *J. Intell. Robot. Syst.*, vol. 86, nos. 3–4, pp. 353–366, Jun. 2017.

[4] I. Hassanzadeh and S. Mobayen, "Controller design for rotary inverted pendulum system using evolutionary algorithms," *Math. Probl. Eng.*, vol. 2011, Aug. 2011, Art. no. 572424.

[5] Y.-F. Chen and A.-C. Huang, "Adaptive control of rotary inverted pendulum system with time-varying uncertainties," *Nonlinear Dyn.*, vol. 76, no. 1, pp. 95–102, Apr. 2014.

[6] J. Lee, R. Mukherjee, and H. K. Khalil, "Output feedback stabilization of inverted pendulum on a cart in the presence of uncertainties," *Automatica*, vol. 54, pp. 146–157, Apr. 2015.

[7] I. Shah and F. U. Rehman, "Smooth second order sliding mode control of a class of underactuated mechanical systems," *IEEE Access*, vol. 6, pp. 7759–7771, Feb. 2018.

[8] M. El-Bardini and A. M. El-Nagar, "Interval type-2 fuzzy PID controller for uncertain nonlinear inverted pendulum system," *ISA Trans.*, vol. 53, pp. 732–743, May 2014.

[9] F. Ding, J. Huang, Y. Wang, J. Zhang, and S. He, "Sliding mode control with an extended disturbance observer for a class of underactuated system in cascaded form," *Nonlinear Dyn.*, vol. 90, no. 4, pp. 2571–2582, Dec. 2017.

[10] R. Rascón, D. Rosas, and D. Hernandez-Balbuena, "Regulation control of an underactuated mechanical system with discontinuous friction and backlash," *Int. J. Appl. Math. Comput. Sci.*, vol. 27, no. 4, pp. 785–797, 2017.

[11] J. Sandoval, R. Kelly, and V. Santibáñez, "Interconnection and damping assignment passivity-based control of a class of underactuated mechanical systems with dynamic friction," *Int. J. Robust Nonlinear Control*, vol. 21, no. 7, pp. 738–751, May 2011.

[12] A. Nejadfard, M. J. Yazdanpanah, and I. Hassanzadeh, "Friction compensation of double inverted pendulum on a cart using locally linear neuro-fuzzy model," *Neural Comput. Appl.*, vol. 22, no. 2, pp. 337–347, Feb. 2013.

[13] D. Xia, L. Wang, and T. Chai, "Neural-network-friction compensation-based energy swing-up control of pendubot," *IEEE Trans. Ind. Electron.*, vol. 61, no. 3, pp. 1411–1423, Mar. 2014.

[14] C. Aguilar-Avelar, R. Rodríguez-Calderón, S. Puga-Guzmán, and J. Moreno-Valenzuela, "Effects of nonlinear friction compensation in the inertia wheel pendulum," *J. Mech. Sci. Technol.*, vol. 31, no. 9, pp. 4425–4433, Sep. 2017.

[15] G. Pujol and L. Acho, "Stabilization of the furuta pendulum with backlash using H_∞-LMI technique: Experimental validation," *Asian J. Control*, vol. 12, no. 4, pp. 460–467, Jul. 2010.

[16] H. A. Yousef, M. Hamdy, and K. Nashed, "$\mathcal{L}_1$ adaptive fuzzy controller for a class of nonlinear systems with unknown backlash-like hysteresis," *Int. J. Syst. Sci.*, vol. 48, no. 12, pp. 2522–2533, 2017.

[17] G. Tao and P. V. Kokotovic, "Adaptive control of plants with unknown dead-zones," *IEEE Trans. Autom. Control*, vol. 39, no. 1, pp. 59–68, Jan. 1994.

[18] T.-S. Wu, M. Karkoub, H. Wang, H.-S. Chen, and T.-H. Chen, "Robust tracking control of MIMO underactuated nonlinear systems with dead-zone band and delayed uncertainty using an adaptive fuzzy control," *IEEE Trans. Fuzzy Syst.*, vol. 25, no. 4, pp. 905–918, Aug. 2017.

[19] G. Tao and F. L. Lewis, Eds., *Adaptive Control of Nonsmooth Dynamic Systems*. New York, NY, USA: Springer-Verlag, 2001.

[20] H. Olsson and K. J. Åström, "Friction generated limit cycles," *IEEE Trans. Control Syst. Technol.*, vol. 9, no. 4, pp. 629–636, Jul. 2001.

[21] R. H. A. Hensen, M. J. G. van de Molengraft, and M. Steinbuch, "Friction induced hunting limit cycles: A comparison between the LuGre and switch friction model," *Automatica*, vol. 39, no. 12, pp. 2131–2137, Dec. 2003.

[22] L. Márton, "On analysis of limit cycles in positioning systems near Striebeck velocities," *Mechatronics*, vol. 18, no. 1, pp. 46–52, Feb. 2008.

[23] S.-L. Chen, K. K. Tan, and S. Huang, "Friction modeling and compensation of servomechanical systems with dual-relay feedback approach," *IEEE Trans. Control Syst. Technol.*, vol. 17, no. 6, pp. 1295–1305, Nov. 2009.

[24] S.-L. Chen, K. K. Tan, and S. Huang, "Limit cycles induced in type-1 linear systems with PID-type of relay feedback," *Int. J. Syst. Sci.*, vol. 40, no. 12, pp. 1229–1239, 2009.

[25] M. M. Z. Shahadat, T. Mizuno, Y. Ishino, and M. Takasaki, "Effect of nonlinearity caused by friction on a negative stiffness control system," *IEEE Trans. Control Syst. Technol.*, vol. 22, no. 4, pp. 1385–1395, Jul. 2014.

[26] M. Landry, S. A. Campbell, K. Morris, and C. O. Aguilar, "Dynamics of an inverted pendulum with delayed feedback control," *SIAM J. Appl. Dyn. Syst.*, vol. 4, no. 2, pp. 333–351, 2005.

[27] A. A. Martynyuk and N. V. Nikitina, "On oscillations of a frictional pendulum," *Int. Appl. Mech.*, vol. 42, no. 2, pp. 214–220, Feb. 2006.

[28] Y. Orlov, L. T. Aguilar, L. Acho, and A. Ortiz, "Asymptotic harmonic generator and its application to finite time orbital stabilization of a friction pendulum with experimental verification," *Int. J. Control*, vol. 81, no. 2, pp. 227–234, 2008.

[29] S. Andary, A. Chemori, and S. Krut, "Control of the underactuated inertia wheel inverted pendulum for stable limit cycle generation," *Adv. Robot.*, vol. 23, no. 15, pp. 1999–2014, 2009.

[30] H. Vasudevan, A. M. Dollar, and J. B. Morrell, "Design for control of wheeled inverted pendulum platforms," *J. Mech. Robot.*, vol. 7, no. 4, pp. 1–12, Nov. 2015.

[31] M. Eom and D. Chwa, "Robust swing-up and balancing control using a nonlinear disturbance observer for the pendubot system with dynamic friction," *IEEE Trans. Robot.*, vol. 31, no. 2, pp. 331–343, Apr. 2015.

[32] V. M. Hernández-Guzmán, M. Antonio-Cruz, and R. Silva-Ortigoza, "Linear state feedback regulation of a Furuta pendulum: Design based on differential flatness and root locus," *IEEE Access*, vol. 4, pp. 8721–8736, Dec. 2016.

[33] A. T. Azar and F. E. Serrano, "Stabilization of mechanical systems with backlash by PI loop shaping," *Int. J. Syst. Dyn. Appl.*, vol. 5, no. 3, pp. 21–46, Jul./Sep. 2016.

[34] B. Armstrong-Hélouvry, P. Dupont, and C. C. De Wit, "A survey of models, analysis tools and compensation methods for the control of machines with friction," *Automatica*, vol. 30, no. 7, pp. 1083–1138, Jul. 1994.

[35] J. Moreno-Valenzuela, C. Aguilar-Avelar, S. A. Puga-Guzmán, and V. Santibáñez, "Adaptive neural network control for the trajectory tracking of the Furuta pendulum," *IEEE Trans. Cybern.*, vol. 46, no. 12, pp. 3439–3452, Dec. 2016.
[36] M. A. Cruz, R. S. Ortigoza, C. M. Sánchez, V. M. H. Guzmán, J. S. Gutiérrez, and J. C. H. Lozada, "Parallel computing as a tool for tuning the gains of automatic control laws," *IEEE Latin Amer. Trans.*, vol. 15, no. 6, pp. 1189–1196, Jun. 2017.
[37] A. Zhang, X. Lai, M. Wu, and J. She, "Nonlinear stabilizing control for a class of underactuated mechanical systems with multi degree of freedoms," *Nonlinear Dyn.*, vol. 89, no. 3, pp. 2241–2253, Aug. 2017.
[38] T. Ortega-Montiel, R. Villafuerte-Segura, and C. Vázquez-Aguilera, and L. Freidovich, "Proportional retarded controller to stabilize underactuated systems with measurement delays: Furuta pendulum case study," *Math. Probl. Eng.*, vol. 2017, Dec. 2017, Art. no. 2505086.
[39] C. Aguilar-Ibáñez and H. Sira-Ramírez, "A linear differential flatness approach to controlling the Furuta pendulum," *IMA J. Math. Control Inf.*, vol. 24, no. 1, pp. 31–45, Mar. 2007.
[40] H. Sira-Ramírez and S. K. Agrawal, *Differentially Flat Systems*. New York, NY, USA: Marcel Dekker, 2004.
[41] J. J. Slotine and W. Li, *Applied Nonlinear Control*. Upper Saddle River, NJ, USA: Prentice-Hall, 1989.
[42] D. J. Block, K. J. Åström, and M. W. Spong, *The Reaction Wheel Pendulum*, 1st ed. River Forest, IL, USA: Morgan & Claypool, 2007.
[43] I. Fantoni and R. Lozano, "Stabilization of the Furuta pendulum around its homoclinic orbit," *Int. J. Control*, vol. 75, no. 6, pp. 390–398, 2002.
[44] I. Fantoni and R. Lozano, *Non-Linear Control for Underactuated Mechanichal Systems*. London, U.K.: Springer-Verlag, 2002.
[45] D. Putra, H. Nijmeijer, and N. van de Wouw, "Analysis of undercompensation and overcompensation of friction in 1DOF mechanical systems," *Automatica*, vol. 43, no. 8, pp. 1387–1394, Aug. 2007.

MAYRA ANTONIO-CRUZ received the B.S. degree in mechatronics from the Instituto Tecnológico de Reynosa, Tamaulipas, Mexico, in 2012, and the M.S. degree in computing technology from the Centro de Innovación y Desarrollo Tecnológico en Cómputo, Instituto Politécnico Nacional, Mexico City, Mexico, in 2015, where she is currently pursuing the Ph.D. degree with the Mechatronics Department.

Her current research interests include the theory and application of automatic control in underactuated mechanical systems and power electronic systems. Also, she is interested in the development of educational technology. During her academic trajectory, she received the Best Academic Performance Award in the cycle of schooling from 2014 to 2015. Also, she was a recipient of the Distinction to Polytechnic Merit: Presea Lázaro Cárdenas 2016, in the Physical and Mathematical Sciences Area at Master level.

VICTOR MANUEL HERNÁNDEZ-GUZMÁN was born in Querétaro, Mexico. He received the B.S. degree in electrical engineering from the Instituto Tecnológico de Querétaro, Querétaro, in 1988, the M.S. degree in electrical engineering from the Instituto Tecnológico de la Laguna, Torreón, Mexico, in 1991, and the Ph.D. degree in electrical engineering from CINVESTAV-IPN, Mexico City, Mexico, in 2003.

He has been a Professor with the Universidad Autónoma de Querétaro, Querétaro, since 1995, where he teaches classical and nonlinear control. He has co-authored the book *Automatic Control: Design Theory, Prototype Construction, Modeling, Identification and Experimental Tests* (in Spanish) (Mexico City, Mexico: Colección CIDETEC-IPN, 2013). He has published over 45 papers in refereed journals. His research interests include control of mechatronic systems, mobile robots, and electro mechanical systems. This includes control of different classes of AC electric motors when actuating on complex nonlinear mechanical loads. He has a particular interest in prototype construction to teach classical and nonlinear control techniques.

RAMÓN SILVA-ORTIGOZA received the B.S. degree in electronics from Benemérita Universidad Autónoma de Puebla, Puebla, Mexico, in 1999, and the M.S. and Ph.D. degrees in electrical engineering (mechatronics) from the Centro de Investigación y de Estudios Avanzados, Instituto Politécnico Nacional (IPN), Mexico City, Mexico, in 2002 and 2006, respectively.

He has been a Researcher with the Department of Mechatronics, Centro de Innovación y Desarrollo Tecnológico en Cómputo, IPN (CIDETEC-IPN), since 2006, and belongs to SNI-CONACYT, Mexico. He has co-authored the book *Control Design Techniques in Power Electronics Devices* (London, U.K.: Springer-Verlag, 2006) and the book *Automatic Control: Design Theory, Prototype Construction, Modeling, Identification and Experimental Tests* (in Spanish) (Mexico City, Mexico: CIDETEC-IPN, 2013). He was an Editor of the book *Mechatronics* (in Spanish) (Mexico City, Mexico: CIDETEC-IPN, 2010). He has published over 45 papers in JCR indexed journals, three chapters in international books, and he has presented over 40 papers in international conferences. He has been an advisor of over 20 postgraduate students and two B.S. students. Four of his students have been honored with the Presea Lázaro Cárdenas Award in 2012, 2015, 2016, and 2018, the most important prize granted by the Instituto Politécnico Nacional of Mexico to its students. Also, two of these students in 2015 and 2017 have also been honored with The Best Master Thesis Award in the Instituto Politécnico Nacional of Mexico. He has been the leader in more than 10 research projects and he has collaborated in nine additional research projects. His research interests include mechatronic control systems, mobile robotics, control in power electronics, and development of educational technology. His research work has been cited over 600 times. He has been a reviewer in several JCR indexed journals. Also, he has been a referee in several awards of research and engineering in Mexico and in the National Program of Quality Postgraduate and research projects of CONACYT.